The transcriptional landscape of the developing chick trigeminal ganglion

Carrie E. Leonard[1], Alec McIntosh[2], Johena Sanyal[1], Lisa A. Taneyhill[1,*]

[1]Department of Animal and Avian Sciences, University of Maryland, College Park, MD 20742 USA

[2]Lombardi Comprehensive Cancer Center, Georgetown University, Washington, DC, 20007 USA

*Corresponding author; Email: ltaney@umd.edu

Keywords: Trigeminal ganglion, neural crest cells, placode cells, RNA-sequencing

Funding information: NIH R01DE024217, R21DE033786

Summary

The trigeminal ganglion is a critical structure in the peripheral nervous system, responsible for transmitting sensations of touch, pain, and temperature from craniofacial regions to the brain. Trigeminal ganglion development depends upon intrinsic cellular programming as well as extrinsic signals exchanged by diverse cell populations. With its complex anatomy and dual cellular origin from cranial placodes and neural crest cells, the trigeminal ganglion offers a rich context for examining diverse biological processes, including cell migration, fate determination, adhesion, and axon guidance. Avian models have, so far, enabled key insights into craniofacial and peripheral nervous system development. Yet, the molecular mechanisms driving trigeminal ganglion formation and subsequent nerve growth remain elusive. In this study, we performed RNA-sequencing at multiple stages of chick trigeminal ganglion development and generated a novel transcriptomic dataset that has been curated to illustrate temporally dynamic gene expression patterns. This publicly available resource identifies major pathways involved in trigeminal gangliogenesis, particularly with respect to the condensation and maturation of placode-derived neurons, thus inviting new lines of research into the essential processes governing trigeminal ganglion development.

Introduction

The trigeminal ganglion is responsible for relaying sensations like touch, pain, and temperature from the face and oral cavity to the central nervous system[1]. Trigeminal nerve dysfunction causes disabling conditions including migraine headache, orofacial pain, and chronic dry eye, whose etiologies remain poorly understood[2–4]. Hereditary disorders associated with cranial sensory deficits are also explained, in part, by altered trigeminal nerve development[5–7]. Despite clear relevance to human health, the genetic landscape and molecular mechanisms underlying trigeminal ganglion neurodevelopment are still poorly characterized.

Peripheral nervous system development begins early during embryogenesis, at stages that are difficult to access in mammals. Avian studies have historically offered critical insight into the cellular lineage and molecular processes that govern cranial gangliogenesis[8–10]. Primary sensory neurons reside in peripheral sensory ganglia which are largely derived from the neural crest, a transient, multipotent progenitor population that gives rise to diverse tissues during

vertebrate embryogenesis[11]. Likewise, cranial ganglia contain neural crest-derived sensory neurons and glia while also receiving neuronal contributions from specialized ectodermal thickenings called placodes[12]. While most cranial ganglia contain either neural crest- or placode-derived neurons that are spatially distinct, the trigeminal ganglion uniquely comprises a mixed neuronal population arising from both lineages[10,13]. Development of a functional trigeminal ganglion relies upon intrinsic transcriptional programming as well as reciprocal communication between neural crest and placode cells[14–17].

Cranial neural crest cells, which originate in the dorsal neural folds and migrate to their final destinations within the embryo, influence the differentiation, migration, and growth of placode cells[18–20]. Chemotactic cues are sent by both neural crest and placode cells to direct their migration to the trigeminal ganglion anlage[21,22]. In tandem, migratory neural crest cells create corridors through which placodal neurons travel after delaminating from the overlying ectoderm[23,24]. Neurogenesis is staggered between the two progenitor populations, such that placode cells are the first to adopt a neuronal fate, followed by neural crest cells, which also give rise to glia, including satellite glial cells within the ganglion and Schwann cells that line the nerves[25,26]. The coalescence and condensation of placodal neurons with undifferentiated neural crest cells to form the ganglion is mediated by cell adhesion molecules including Cadherins[27,28], and signaling pathways, like Wnt and Slit/Robo[28–30]. Once the earliest trigeminal sensory axons extend from placodal neurons, their growth toward craniofacial sites of innervation is further guided by diffusible factors, such as BMPs[31], semaphorins[32,33], and neurotrophins[34,35]. Thus, the developing trigeminal ganglion and its required interactions between neural crest cells and placodal neurons offer a rich context in which to investigate core biological processes, from fate determination to cell migration to axon guidance.

From decades of elegant work conducted in vertebrate embryos, there is a strong foundational understanding of neural crest and placode cell interactions and their contributions to cranial ganglia[36,37]. However, studies characterizing neurodevelopment from placodes are underrepresented compared to our knowledge of neural crest-derived neurons[38]. The early development and lack of genetic tools to target specific placodal subpopulations in mammalian models hinders research progress in this area. In contrast, chick embryos offer relative ease of access to facilitate the experimental manipulation of neural crest and distinct placodal progenitors[39], with the additional benefit of continued development *in ovo*. With the evolutionary conservation of developmental mechanisms between species[37,40,41], the chick embryo remains a

84 favored, economical model for examining embryonic development, including the formation of
85 neurogenic cranial placodes.

86 To elucidate normal gene expression dynamics during trigeminal ganglion development,
87 we performed RNA-sequencing at sequential timepoints and curated a novel transcriptomic
88 dataset to illustrate relative changes in gene expression over time. Raw and processed data are
89 available in Gene Expression Omnibus (NCBI) under Accession #GSE282770 to encourage
90 further exploration by researchers interested in craniofacial and/or peripheral nervous system
91 development. Our findings identify key pathways involved in trigeminal gangliogenesis and
92 provide critical insight into the molecular mechanisms underlying neurodevelopment and cellular
93 interactions between placode-derived neurons and neural crest cells.

94 **Methods**

95 *Collection of chicken embryos and trigeminal ganglia*

96 Fertilized chicken eggs (*Gallus gallus*) were procured from Hy-Line North America
97 (Elizabethtown, PA) or Centurion Poultry (Lexington, GA) and incubated in a humid environment
98 at 37°C. Embryos were staged using the Hamburger-Hamilton (HH) method[42], then removed
99 from the egg and placed into sterile, ice-cold Ringer's solution (0.125M sodium chloride, 1.5mM
100 calcium chloride dihydrate, 5mM potassium chloride, 0.8mM sodium phosphate dibasic,
101 adjusted to pH 7.4). Trigeminal ganglia were dissected using electrolytically sharpened tungsten
102 needles, pooled by appropriate stages, and flash frozen in liquid nitrogen until total RNA
103 extraction. With three pooled biological replicates for each stage, a total of 47 ganglia were used
104 from HH13/14 embryos, 47 ganglia from HH15/16 embryos, and 56 ganglia from HH17/18
105 embryos. For immunohistochemical studies, HH17/18 embryos were collected and fixed with
106 gentle agitation in 4% paraformaldehyde for 2 hours at room temperature, then washed 3 times
107 for 10 minutes each in 1× PBS/0.1% Triton X-100 (Tx-100).

108 *RNA extraction, library preparation, RNA-sequencing and data processing*

109 Total RNA was isolated according to the manufacturer's protocol for the RNAqueous
110 Total RNA Isolation kit (ThermoFisher, #AM1912). RNA concentration and integrity were
111 quantified with Nanodrop (ThermoFisher) and Agilent 2100 bioanalyzer. The TruSeq sample
112 preparation kit (Illumina) was used to generate poly(A)-enriched cDNA libraries, followed by
113 assessment of quality and quantity using the bioanalyzer. 100bp paired-end reads were
114 obtained with the Illumina HiSeq 1500 platform. Illumina adapter sequences were removed

using Trimmomatic[43] and the quality of reads assessed with FastQC[44]. HISAT2[45] was used to align reads with a *Gallus gallus* reference genome (bGalGal1.mat.broiler.GRCg7b) and the number of reads per gene was quantified using HTSeq[46]. For principal component analysis, sample variability was calculated and visualized after normalization in R. Differential expression analyses were performed on normalized counts using DESeq2[47], with three biological replicates from pooled trigeminal ganglia per indicated stage bin, and two technical replicates per biological replicate included. Heatmaps were generated using the online tool Morpheus from the Broad Institute (https://software.broadinstitute.org/morpheus/). Raw and processed data were deposited in Gene Expression Omnibus (NCBI) under Accession #GSE282770.

Polar plot and Gene Ontology enrichment analyses

Normalized differential expression data were first used to calculate "H" by transforming sequential data (T^0-T^1-T^2) into angular values representing relative gene expression at HH13/14 (T^0), HH15/16 (T^1), and HH17/18 (T^2), respectively[48,49]. The determined angular values illustrate expression dynamics (i.e., low-low-high) on a radial plot. "H" corresponds to the relative angular position of individual gene expression across T^0-T^1-T^2 (i.e., yellow; H=0 degrees indicates no change from T^0-T^1, and a significant increase in gene expression from T^1-T^2). MaxLog, as determined with DESeq2 as the maximal Log_2 fold change between any two timepoints, is illustrated in the polar plot as distance from the center, while the transparency of a particular point reflects the average normalized gene expression of a given gene (i.e., values greater than 100 are fully opaque whereas lower averages are more transparent). Polar plots were generated with *ggplot2*[50] and scaled expression profiles were created in R using previously described equations[51] adapted from the Mandrup group[48,49]. Briefly, relative mean changes in gene expression were transformed to an angle between -180 and +180 degrees, then further transformed to a scale from 0 to 360 degrees, which was used to determine color based on degree. Differentially expressed genes were plotted using polar coordinates with the radius equal to MaxLog, and angular position around the radial plot determined by the change trend. Color-coded, three-point profile annotations demonstrating relative expression changes corresponding from left to right as HH13/14 (T^0), HH15/16 (T^1), and HH17/18 (T^2), respectively, are displayed every 30 degrees along the outer edge of the polar plot. For Gene Ontology (GO) enrichment, genes were parsed into six sectors by grouping profiles into 60-degree intervals starting at 0 degrees, which denotes genes that were unchanged between T^0-T^1, but significantly increased from T^1-T^2. Using *EnrichR*[52–54], genes within each 60-degree sector were assessed against the GO Biological Process and GO Cellular Compartment databases[55]. Prism

148 (Graphpad) was used to graph the top fifteen pathways most enriched for each sector based on
149 p-value. Excel files summarizing all color-matched calculated values for the polar plot and
150 sector-parsed GO analyses are included as supplemental files.

151 *Embedding, cryosectioning, immunohistochemistry, and in situ hybridization data*

152 Fixed embryos were processed through a sucrose gradient by submerging in 1× PBS
153 plus 5% sucrose (w/v) for 10 minutes, followed by 1× PBS plus 15% sucrose (w/v) overnight at
154 4°C. Embryos were then incubated in 1× PBS plus 7.5% gelatin (w/v) and 15% sucrose at 37°C
155 for 3 hours, before transfer into a solution of 1× PBS plus 20% gelatin (w/v) and 15% sucrose
156 and incubation overnight at 37°C in a humidified incubator. Gelatin-equilibrated embryos were
157 then embedded in 1× PBS plus 20% gelatin and flash frozen in liquid nitrogen vapor. Embedded
158 embryos were sectioned at 12μm on a cryostat at -25°C, and tissue sections were collected on
159 Superfrost Plus charged slides (VWR, Cat. No. 48311-703). Slides were de-gelatinized in 1×
160 PBS at 42°C for 15 minutes, then rinsed in 1× PBS at room temperature before permeabilization
161 in 1× PBS/0.5% Tx-100 for 10 minutes. Tissue was blocked with 10% (v/v) heat-treated sheep
162 serum (HTSS, Sigma) in 1×PBS/0.1% Tx-100 for 1 hour at room temperature in a humidified
163 chamber. Primary antibodies were diluted in 1× PBS/0.1% Tx-100 plus 5% HTSS and applied
164 overnight at 4°C using the following concentrations: Sox10 (1:100, Cat. No. 66786-1-Ig,
165 Proteintech); Islet1 (1:100, Cat. No. 40.2D6, DSHB); STMN2 (1:100, Cat. No. 720178,
166 ThermoFisher); beta III Tubulin ("Tubb3", 1:500, Cat. No. AB78078, Abcam); N-Cadherin (1:100,
167 Cat. No. AB18203, Abcam); and HuC/D (1:100, Cat. No. A-21271, ThermoFisher). The following
168 day, tissue sections were washed 4 times for 30 minutes each at room temperature in 1×
169 PBS/0.1% Tx-100. Fluorescently labeled secondary antibodies (ThermoFisher: goat anti-mouse
170 IgG_1 Cat. No. A-21125 or A-21240, goat anti-mouse IgG_{2a} Cat. No. A-21131, goat anti-mouse
171 IgG_{2b} Cat. No. A-21145, goat anti-rabbit Cat No. A-11034 or A-21245; and Southern Biotech:
172 goat anti-mouse IgG_{2a} Cat. No. 1080-31) were diluted at 1:500 in 1× PBS/0.1% Tx-100 plus 5%
173 HTSS and applied overnight at 4°C in a humidified chamber. Slides were washed as described
174 above for the primary antibodies, and coverslips mounted using DAPI Fluoromount-G Mounting
175 Medium (Southern Biotech, Cat. No. 0100-20). Images were acquired and processed using a
176 Zeiss LSM 800 confocal microscope with Zen Blue software (Zeiss). *In situ* hybridization data
177 from the developing trigeminal ganglion in embryonic day (E)11.5 mouse was obtained from the
178 Allen Developing Mouse Brain Atlas[56].

179

Results and Discussion

To elucidate gene expression dynamics and identify key molecular drivers of trigeminal ganglion development, we performed a bulk RNA-sequencing time course assay. Trigeminal ganglia were collected from chicken embryos, pooled into three Hamburger-Hamilton (HH) stage-dependent bins[42] (HH13/14, HH15/16, or HH17/18), and separated into three biological replicates per bin before RNA extraction and sequencing. A total of 47 trigeminal ganglia were used from HH13/14 embryos, corresponding to a time when placodal neurons and neural crest cells begin to coalesce within the trigeminal ganglion anlage. HH15/16 trigeminal ganglia (n=47) are in the process of condensing into a compact structure, comprising a mixture of neural crest cells and placodal neurons that have initiated neurite extension. By HH17/18 (n=56), the trigeminal ganglion is densely populated with placodal neurons that are actively undergoing axon growth and guidance, comingled with neural crest cells that have not yet differentiated into neurons or glia[12,57,58]. Principal component analysis of normalized gene counts revealed samples generally clustered according to developmental stage, with HH13/14 trigeminal ganglia least similar to HH17/18 trigeminal ganglia, and HH15/16 trigeminal ganglia falling in between the distributions of HH13/14 and HH17/18 samples (Supplemental Figure 1A). Our goal was not only to detect differentially expressed genes at each stage, but to visualize the dynamic patterns spanning these three developmental timepoints. To this end, polar plots were created to summarize the relative relationships of individual genes from HH13/14 to HH15/16 to HH17/18, and cluster genes into groups based on similar temporal profiles (Figure 1)[48,49].

In total, 14,506 genes were detected across the three timepoints. 5,703 genes exhibited significant differential expression ($p<0.05$ after Benjamini-Hochberg correction, see Supplemental File 1) at one timepoint compared to at least one other and were included in the polar plot (Figure 1A) and associated histogram (Figure 1B). The upregulation or downregulation of individual differentially expressed genes from HH13/14 to HH15/16 to HH17/18 was transformed into angular representations of relative expression over time, and placed onto a circular spectrum, where position around the circle is analogous to angular expression profiles, which are color-coded based on the degree within the circle, i.e., 0 degrees (yellow) is analogous to no change between HH13/14 and HH15/16, then a significant increase from HH15/16 to HH17/18 (Figure 1A). Of the differentially expressed genes, there were 765 with a maximal Log_2 fold change (MaxLog) greater than 1.0, 124 genes with MaxLog greater than 2.0, and 14 genes with MaxLog exceeding 4.0 in any comparison, as indicated by increasing distance from the center of the polar plot (Figure 1A). Generally, the greatest

213 changes in expression occurred in those genes exhibiting a temporal profile with upregulation
214 between HH13/14 and HH15/16 (green to blue on polar plot), and either upregulation (yellow to
215 green on polar plot) or sustained expression (green to blue on polar blot) from HH15/16 to
216 HH17/18 (Figure 1A). The greatest numbers of differentially expressed genes occurred between
217 0 and +60 degrees (yellow to green) and between -120 and -180 degrees (indigo to purple) on
218 the polar plot (Figure 1B), suggesting most changes in gene expression are unidirectional
219 and/or sustained over time, regardless of increased versus decreased expression.

220 To understand how shared temporal gene expression profiles relate to biological events
221 occurring in the developing trigeminal ganglion from HH13/14 to HH17/18, and to identify which
222 genes may play a role in these processes, the polar plot was divided into 60-degree sectors.
223 Differentially expressed genes within any given 60-degree sector displayed similar expression
224 trajectories, on average, and were assessed for Gene Ontology (GO) enrichment against the
225 GO: Biological Processes and GO: Cellular Component databases[55] (Figures 2-4, Supplemental
226 Figures 2-5, Supplemental File 2).

227 Within Sector 1, 1900 genes exhibited expression profiles that, on average, increased
228 consistently from HH13/14 to HH15/16 and from HH15/16 to HH17/18, with some variation at
229 the mid-point, but consistent upregulation by HH17/18 when compared to HH13/14 (Figure 2A
230 and 2B). Significant biological processes and cellular components associated with Sector 1
231 genes included “Axonogenesis”, “Axon Guidance”, “Positive Regulation of Neuron Projection
232 Development”, “Neuron Projection”, “Axon”, and “Cytoskeleton” (Figure 2C and 2D). Heatmaps
233 illustrating relative temporal expression of differentially expressed genes associated with the
234 regulation of axonogenesis revealed that, as expected, temporal expression patterns largely
235 segregate according to sector. Further, the vast majority of genes associated with
236 axonogenesis-related GO terms fall under Sector 1 (Supplemental Figure 1B). These findings
237 align with the ongoing arrival and maturation of placodal neurons in the trigeminal ganglion
238 between HH13/14 and HH17/18.

239 Indeed, we confirmed the presence of Sox10-positive neural crest cells and Islet1-
240 positive placodal neurons in the HH18 trigeminal ganglion (Figure 3A). We also observed Sector
241 1 gene protein products, Stmn2 and Elavl4 (also known as HuD), in placodal neurons that
242 expressed beta III tubulin or N-Cadherin (Figure 3B-C). Moreover, Sector 1 comprises several
243 neuronal genes shown to be highly expressed in the developing mouse and chick trigeminal
244 ganglion that play critical roles in axonal growth and maintenance, including *Ntrk1*, *Robo2*, and
245 *Cntn2* (Figure 3D)[28,29,56,59–61]. While other signaling pathways known to be involved in sensory

246 axon growth and guidance were among the upregulated genes in Sector 1, including Eph
247 receptors, Semaphorins, and Notch (Figure 2C, right panel), genes within these families have
248 not been well characterized in the trigeminal ganglion. Additionally, the GO enrichment results
249 indicated changes in cell migration, cell signaling, and interactions with the extracellular matrix
250 (Figure 2C and 2D). Such molecular changes may reflect migration dynamics of placodal
251 neurons and/or neural crest cells as they populate the trigeminal ganglion and mature over time.
252 They may also reflect genes important for sensing the environment as axons grow in search of
253 target tissues, or as undifferentiated neural crest cells process extracellular cues that may
254 influence their eventual fate.

255 In Sector 2, 796 genes, on average, were upregulated at HH15/16 compared to
256 HH13/14, with sustained, but not further increased, expression at HH17/18 (Figure 4A and 4B).
257 Differential expression of Sector 2 genes reflected activation of pathways involved in autophagy,
258 as evidenced by enrichment in categories including “Lysosomal Transport”, “Positive Regulation
259 of Autophagy”, “Vesicle-Mediated Transport”, “Lysosome”, “Recycling Endosome”, and
260 “Autophagosome” (Figure 4C and 4D). While autophagy is a key player in processes including
261 migration and differentiation that could be occurring in multiple cell types, it is also essential for
262 proper neuronal development, plasticity, and survival[62,63]. Indeed, several neurodevelopmental
263 disorders associated with sensory deficits, including autism spectrum disorders, are linked to
264 dysfunctional autophagy[64]. Little has been described regarding the role of autophagy in
265 trigeminal ganglion neurodevelopment, yet our findings indicate a large proportion of
266 differentially expressed genes may participate in this process as placodal neurons mature.
267 While genes identified in Sectors 1 and 2 are largely associated with neurodevelopmental
268 mechanisms, it is also plausible that they are driven by transcriptional changes in neural crest
269 cells or even cranial mesenchyme, as multiple populations are present in our samples. Follow-
270 up studies are needed to determine the unique cellular localization of differentially expressed
271 transcripts, and how the identified pathways may function in placodal neurons versus neural
272 crest cells at the examined timepoints.

273 Overall, genes in Sector 3 were associated with temporary upregulation of processes
274 involved in sensory perception, glucose and ion transport, homeostasis, and cytoskeletal
275 reorganization at HH15/16 (Supplemental Figure 2). Such processes are important for cell-cell
276 communication, which is critical as undifferentiated neural crest cells and placodal neurons
277 further condense to generate the ganglion, including supporting morphological changes in both
278 cell populations[65–67]. Downregulated genes in Sectors 4 and 5 that remained lower at HH17/18

279 were generally associated with negative regulation of gene expression and protein biogenesis
280 (Supplemental Figures 3-4). These findings may mirror trigeminal ganglion cells as they
281 transition from proliferative and/or migratory progenitor states into cells with more defined fates,
282 such as the increasing number of post-mitotic placodal neurons in the trigeminal ganglion over
283 time, or neural crest cells that are preparing to differentiate into glia and/or neurons. Finally, the
284 expression profiles of genes in Sector 6 generally reflected a temporary decrease in
285 mitochondrial metabolic processes and cell motility (Supplemental Figure 5). This pattern may,
286 too, reflect a pause and restructuring of energy-dependent cellular processes needed to support
287 later steps in gangliogenesis, including axon extension and transport for neurodevelopment[68,69].
288 These non-exhaustive hypotheses require further investigation in order to fully understand the
289 implications of individual gene expression trends in specific cell types.

290 Interpretation of our data is limited by the inability to assign changes in individual gene
291 expression to a particular cell population. The RNA-sequencing data were generated from
292 whole trigeminal ganglion lysate and, therefore, encompasses both placodal neurons and neural
293 crest cells. Moreover, tissue samples likely included some contamination from the surrounding
294 mesenchyme, especially at stages that precede trigeminal ganglion condensation. Given the
295 migratory nature of several cell populations during the examined stages of craniofacial
296 development, it is also possible that some transient changes in gene expression (for example,
297 genes in Sectors 3 or 6) are explained by cells in transit to other tissues that do not ultimately
298 remain in the trigeminal ganglion.

299 Even with these limitations, advantages of our bulk sequencing approach in comparison
300 to single-cell or cell-sorted analyses include higher sensitivity and fewer gene "dropout events",
301 thus providing a more complete profile of average gene expression over time, which can be
302 compared against more filtered data sets[70,71]. For example, Patthey et al. (2016) previously
303 examined transcript expression in cranial sensory neurons by pre-selecting for mature neurons
304 that expressed Neurofilament protein[58]. Our data confirmed the presence of neuronal genes
305 deemed specific to the trigeminal ganglion, including *Prdm12*, *Gad2*, *Chrna3*, *Chrnb4*, and *Tox2*
306 (Supplemental File 1)[58]. However, we also detected several genes in trigeminal ganglion lysate
307 that Patthey et al. determined to be specific to neurons in other cranial ganglia, including *Esrrg*,
308 *Irx2*, *Pdzrn4*, *Sult4a1*, *Shox2*, and *Lhx4* (Supplemental File 1)[58]. It is possible that these genes
309 are instead expressed in non-neuronal cells within our trigeminal ganglion samples and,
310 therefore, would have been selected against in Patthey et al. However, *Shox2* and *Lhx4*, for
311 example, have established roles in sensory neuron development[72,73]. Moreover, our data

312 capture genes that are expressed in newly differentiated, immature placodal neurons that would
313 not yet express Neurofilament protein. Therefore, it is useful to consider filtered and bulk
314 datasets together in order to draw and evaluate conclusions. In either case, RNA-sequencing,
315 while informative, does not account for post-transcriptional or post-translational mechanisms
316 that control gene expression. Follow-up assessment of protein products compared to their
317 respective transcript profiles would provide additional insight into the functional consequences
318 of the described transcriptional dynamics.

319

320 **Conclusions**

321 Our report visually and quantitatively illustrates temporal dynamics in gene expression,
322 cellular events, and key molecular pathways that participate in the development of the trigeminal
323 ganglion in chick. These gene signatures correspond to key stages in trigeminal gangliogenesis,
324 from the time when neural crest and placode cells coalesce and form a cohesive structure,
325 through the neuronal maturation and early axon extension of placodal neurons. This novel,
326 publicly available dataset is processed and curated with the goal of inspiring new lines of
327 investigation into the molecular mechanisms underlying cranial sensory neuron development
328 and the cellular interactions required for proper craniofacial development during embryogenesis.

329

330 **Acknowledgements**

331 We thank Chyong-Yi Wu, Ph.D. for technical assistance in sample preparation. We thank
332 Sue Zhao, Ph.D, Hector Corrada Bravo, Ph.D., and the UMD Institute for Bioscience &
333 Biotechnology Research for their technical assistance and expertise in sequencing and
334 preliminary data analyses.

335

336

337

338 **References**

339 1. Sanders, R. D. The Trigeminal (V) and Facial (VII) Cranial Nerves: Head and Face Sensation and
340 Movement. *Psychiatry (Edgmont)* **7**, 13–6 (2010).

2. Olesen, J., Burstein, R., Ashina, M. & Tfelt-Hansen, P. Origin of pain in migraine: evidence for peripheral sensitisation. *The Lancet Neurology* vol. 8 679–690 Preprint at https://doi.org/10.1016/S1474-4422(09)70090-0 (2009).

3. Soares, F. *et al.* Effect of Genetic Polymorphisms on Pain Sensitivity in the Orofacial Region: A Systematic Review. *J Oral Facial Pain Headache* **34**, 353–363 (2020).

4. Patel, S., Hwang, J., Mehra, D. & Galor, A. Corneal Nerve Abnormalities in Ocular and Systemic Diseases. *Exp Eye Res* **202**, 108284 (2021).

5. Leonard, C. E., Quiros, J., Lefcort, F. & Taneyhill, L. A. Loss of Elp1 disrupts trigeminal ganglion neurodevelopment in a model of familial dysautonomia. *Elife* **11**, (2022).

6. Karpinski, B. A. *et al.* Selective disruption of trigeminal sensory neurogenesis and differentiation in a mouse model of 22q11.2 deletion syndrome. *DMM Disease Models and Mechanisms* **15**, (2022).

7. Schwartzlow, C. & Kazamel, M. Hereditary Sensory and Autonomic Neuropathies: Adding More to the Classification. *Curr Neurol Neurosci Rep* **19**, (2019).

8. Le Douarin, N. M. The avian embryo as a model to study the development of the neural crest: A long and still ongoing story. *Mechanisms of Development* vol. 121 1089–1102 Preprint at https://doi.org/10.1016/j.mod.2004.06.003 (2004).

9. Méndez-Maldonado, K., Vega-López, G. A., Aybar, M. J. & Velasco, I. Neurogenesis From Neural Crest Cells: Molecular Mechanisms in the Formation of Cranial Nerves and Ganglia. *Frontiers in Cell and Developmental Biology* vol. 8 Preprint at https://doi.org/10.3389/fcell.2020.00635 (2020).

10. Hamburger, V. Experimental analysis of the dual origin of the trigeminal ganglion in the chick embryo. *Journal of Experimental Zoology* **148**, 91–123 (1961).

11. Bronner, M. E. & LeDouarin, N. M. Development and evolution of the neural crest: An overview. *Developmental Biology* vol. 366 2–9 Preprint at https://doi.org/10.1016/j.ydbio.2011.12.042 (2012).

12. D'Amico-Martel, A. & Noden, D. M. Contributions of placodal and neural crest cells to avian cranial peripheral ganglia. *Am J Anat* **166**, 445–468 (1983).

13. Lwigale, P. Y. Embryonic origin of avian corneal sensory nerves. *Dev Biol* **239**, 323–337 (2001).

14. Moody, S. A. & LaMantia, A.-S. Transcriptional Regulation of Cranial Sensory Placode Development. in *Curr Top Dev Biol* vol. 111 301–350 (2015).

15. Wu, C. Y. & Taneyhill, L. A. Cadherin-7 mediates proper neural crest cell–placodal neuron interactions during trigeminal ganglion assembly. *Genesis* **57**, 1–14 (2019).

16. Wu, C. Y., Hooper, R. M., Han, K. & Taneyhill, L. A. Migratory neural crest cell αN-catenin impacts chick trigeminal ganglia formation. *Dev Biol* **392**, 295–307 (2014).

17. Halmi, C. A., Wu, C. Y. & Taneyhill, L. A. Neural crest cell-placodal neuron interactions are mediated by Cadherin-7 and N-cadherin during early chick trigeminal ganglion assembly. *F1000Res* **11**, 741 (2022).

18. Steventon, B., Mayor, R. & Streit, A. Neural crest and placode interaction during the development of the cranial sensory system. *Dev Biol* **389**, 28–38 (2014).

19. Theveneau, E. & Mayor, R. Neural crest delamination and migration: From epithelium-to-mesenchyme transition to collective cell migration. *Developmental Biology* vol. 366 34–54 Preprint at https://doi.org/10.1016/j.ydbio.2011.12.041 (2012).

20. Leonard, C. E. & Taneyhill, L. A. The road best traveled: Neural crest migration upon the extracellular matrix. *Seminars in Cell and Developmental Biology* vol. 100 177–185 Preprint at https://doi.org/10.1016/j.semcdb.2019.10.013 (2020).

21. Gammill, L. S., Gonzalez, C., Gu, C. & Bronner-Fraser, M. Guidance of trunk neural crest migration reguires neuropilin 2/semaphorin 3F signaling. *Development* **133**, 99–106 (2006).

22. Guidato, S. & Itasaki, N. Wise retained in the endoplasmic reticulum inhibits Wnt signaling by reducing cell surface LRP6. *Dev Biol* **310**, 250–263 (2007).

23. Freter, S., Fleenor, S. J., Freter, R., Liu, K. J. & Begbie, J. Cranial neural crest cells form corridors prefiguring sensory neuroblast migration. *Development (Cambridge)* **140**, 3595–3600 (2013).

24. Barlow, L. A. *Cranial Nerve Development: Placodal Neurons Ride the Crest*. *Current Biology* vol. 12 (2002).

25. Noden', D. M. *An Analysis of the Migratory Behavior of Avian Cephalic Neural Crest Cells'*. *DEVELOPMENTAL BIOLOGY* vol. 42 (1975).

26. D'amico-Martel, A. & Noden, D. An autoradiographic analysis of the development of the chick trigeminal ganglion. *J Embryol Exp Morphol* **55**, 167–182 (1980).

27. Wu, C. Y. & Taneyhill, L. A. Cadherin-7 mediates proper neural crest cell–placodal neuron interactions during trigeminal ganglion assembly. *Genesis* **57**, 1–14 (2019).

28. Shiau, C. E. & Bronner-Fraser, M. N-cadherin acts in concert with Slit1-Robo2 signaling in regulating aggregation of placode-derived cranial sensory neurons. *Development* **136**, 4155–4164 (2009).

29. Shiau, C. E., Lwigale, P. Y., Das, R. M., Wilson, S. A. & Bronner-Fraser, M. Robo2-Slit1 dependent cell-cell interactions mediate assembly of the trigeminal ganglion. *NATURE NEUROSCIENCE VOLUME* **11**, (2008).

30. Shigetani, Y. *et al.* Wise promotes coalescence of cells of neural crest and placode origins in the trigeminal region during head development. *Dev Biol* **319**, 346–358 (2008).

31. Hodge, L. K. *et al.* Retrograde BMP Signaling Regulates Trigeminal Sensory Neuron Identities and the Formation of Precise Face Maps. *Neuron* **55**, 572–586 (2007).

411 32. William Rochlin, M. & Farbman, A. I. *Trigeminal Ganglion Axons Are Repelled By Their*
412 *Presumptive Targets*. (1997).

413 33. Chen, H. *et al.* Neuropilin-2 Regulates the Development of Select Cranial and Sensory Nerves and
414 Hippocampal Mossy Fiber Projections. *Neuron* **25**, 43–56 (2000).

415 34. O'Connor, R. & Tessier-Lavigne, M. Identification of Maxillary Factor, a Maxillary Process–Derived
416 Chemoattractant for Developing Trigeminal Sensory Axons. *Neuron* **24**, 165–178 (1999).

417 35. Enokido, Y., Wyatt, S. & Davies, A. M. Developmental changes in the response of trigeminal
418 neurons to neurotrophins: Influence of birthdate and the ganglion environment. *Development*
419 **126**, 4365–4373 (1999).

420 36. Steventon, B., Mayor, R. & Streit, A. Neural crest and placode interaction during the development
421 of the cranial sensory system. *Dev Biol* **389**, 28–38 (2014).

422 37. York, J. R., Yuan, T. & McCauley, D. W. Evolutionary and Developmental Associations of Neural
423 Crest and Placodes in the Vertebrate Head: Insights From Jawless Vertebrates. *Frontiers in*
424 *Physiology* vol. 11 986 Preprint at https://doi.org/10.3389/fphys.2020.00986 (2020).

425 38. Méndez-Maldonado, K., Vega-López, G. A., Aybar, M. J. & Velasco, I. Neurogenesis From Neural
426 Crest Cells: Molecular Mechanisms in the Formation of Cranial Nerves and Ganglia. *Front Cell Dev*
427 *Biol* **8**, (2020).

428 39. Xu, H., Dude, C. M. & Baker, C. V. H. Fine-grained fate maps for the ophthalmic and
429 maxillomandibular trigeminal placodes in the chick embryo. *Dev Biol* **317**, 174–186 (2008).

430 40. Kee, Y., Byung, J. H., Sternberg, P. W. & Bronner-Fraser, M. Evolutionary conservation of cell
431 migration genes: From nematode neurons to vertebrate neural crest. *Genes Dev* **21**, 391–396
432 (2007).

433 41. Yajima, H. *et al.* Six1 is a key regulator of the developmental and evolutionary architecture of
434 sensory neurons in craniates. *BMC Biol* **12**, 1–18 (2014).

435 42. Hamburger, V. & Hamilton, H. L. A series of normal stages in the development of the chick
436 embryo. *J Morphol* **88**, 49–92 (1951).

437 43. Bolger, A. M., Lohse, M. & Usadel, B. Trimmomatic: A flexible trimmer for Illumina sequence data.
438 *Bioinformatics* **30**, 2114–2120 (2014).

439 44. Andrews, S. FastQC: A quality control tool for high throughput sequence data [Online]. Available
440 online at http://www.bioinformatics.babraham.ac.uk/projects/fastqc/. (2010).

441 45. Kim, D., Langmead, B. & Salzberg, S. L. HISAT: A fast spliced aligner with low memory
442 requirements. *Nat Methods* **12**, 357–360 (2015).

443 46. Anders, S., Pyl, P. T. & Huber, W. HTSeq-A Python framework to work with high-throughput
444 sequencing data. *Bioinformatics* **31**, 166–169 (2015).

445 47. Love, M. I., Huber, W. & Anders, S. Moderated estimation of fold change and dispersion for RNA-
446 seq data with DESeq2. *Genome Biol* **15**, (2014).

48. Siersbfk, R. *et al.* Extensive chromatin remodelling and establishment of transcription factor hotspots during early adipogenesis. *EMBO Journal* **30**, 1459–1472 (2011).

49. Madsen, J. G. S. *et al.* Highly interconnected enhancer communities control lineage-determining genes in human mesenchymal stem cells. *Nat Genet* **52**, 1227–1238 (2020).

50. Wickham, H. ggplot2: Elegant graphics for data analysis. Springer-Verlag New York. ISBN 978-3-319-24277-4, https://ggplot2.tidyverse.org. (2016).

51. Nasir, A. *et al.* The integration of Tgfβ and Egfr signaling programs confers the ability to lead heterogeneous collective invasion. *bioRxiv* 2020.11.14.383232 (2023) doi:10.1101/2020.11.14.383232.

52. Xie, Z. *et al.* Gene Set Knowledge Discovery with Enrichr. *Curr Protoc* **1**, (2021).

53. Chen, E. Y. *et al. Enrichr: Interactive and Collaborative HTML5 Gene List Enrichment Analysis Tool*. http://amp.pharm.mssm.edu/Enrichr. (2013).

54. Kuleshov, M. V. *et al.* Enrichr: a comprehensive gene set enrichment analysis web server 2016 update. *Nucleic Acids Res* **44**, W90–W97 (2016).

55. Aleksander, S. A. *et al.* The Gene Ontology knowledgebase in 2023. *Genetics* **224**, (2023).

56. Allen Institute for Brain Science. Allen Developing Mouse Brain Atlas. *Available from developingmouse.brain-map.org* (2024).

57. McCabe, K. L., Sechrist, J. W. & Bronner-Fraser, M. Birth of ophthalmic trigeminal neurons initiates early in the placodal ectoderm. *Journal of Comparative Neurology* **514**, 161–173 (2009).

58. Patthey, C. *et al.* Identification of molecular signatures specific for distinct cranial sensory ganglia in the developing chick. *Neural Dev* **11**, 1–20 (2016).

59. Ratié, L., Ware, M., Jagline, H., David, V. & Dupé, V. Dynamic expression of Notch-dependent neurogenic markers in the chick embryonic nervous system. *Front Neuroanat* **8**, (2014).

60. Huang, E. J. *et al.* POU domain factor Brn-3a controls the differentiation and survival of trigeminal neurons by regulating Trk receptor expression. *Development* **126**, 2869–2882 (1999).

61. Huang, E. J. *et al.* POU domain factor Brn-3a controls the differentiation and survival of trigeminal neurons by regulating Trk receptor expression. *Development* **126**, 2869–2882 (1999).

62. Allen, E. A. & Baehrecke, E. H. Autophagy in animal development. *Cell Death and Differentiation* vol. 27 903–918 Preprint at https://doi.org/10.1038/s41418-020-0497-0 (2020).

63. Valencia, M., Kim, S. R., Jang, Y. & Lee, S. H. Neuronal autophagy: Characteristic features and roles in neuronal pathophysiology. *Biomolecules and Therapeutics* vol. 29 605–614 Preprint at https://doi.org/10.4062/BIOMOLTHER.2021.012 (2021).

64. Deng, Z., Zhou, X., Lu, J. H. & Yue, Z. Autophagy deficiency in neurodevelopmental disorders. *Cell and Bioscience* vol. 11 Preprint at https://doi.org/10.1186/s13578-021-00726-x (2021).

481 65. Putra, V. D. L., Kilian, K. A. & Knothe Tate, M. L. Biomechanical, biophysical and biochemical
482 modulators of cytoskeletal remodelling and emergent stem cell lineage commitment.
483 *Communications Biology* vol. 6 Preprint at https://doi.org/10.1038/s42003-022-04320-w (2023).

484 66. Shellard, A. & Mayor, R. Integrating chemical and mechanical signals in neural crest cell migration.
485 *Curr Opin Genet Dev* **57**, 16–24 (2019).

486 67. Roycroft, A. *et al.* Redistribution of Adhesive Forces through Src/FAK Drives Contact Inhibition of
487 Locomotion in Neural Crest. *Dev Cell* **45**, 565-579.e3 (2018).

488 68. Smith, G. M. & Gallo, G. The role of mitochondria in axon development and regeneration.
489 *Developmental Neurobiology* vol. 78 221–237 Preprint at https://doi.org/10.1002/dneu.22546
490 (2018).

491 69. Vaarmann, A. *et al.* Mitochondrial biogenesis is required for axonal growth. *Development*
492 *(Cambridge)* **143**, 1981–1992 (2016).

493 70. Yamawaki, T. M. *et al.* Systematic comparison of high-throughput single-cell RNA-seq methods for
494 immune cell profiling. *BMC Genomics* **22**, (2021).

495 71. Chen, G., Ning, B. & Shi, T. Single-cell RNA-seq technologies and related computational data
496 analysis. *Frontiers in Genetics* vol. 10 Preprint at https://doi.org/10.3389/fgene.2019.00317
497 (2019).

498 72. Guo, R. *et al.* LIM Homeobox 4 (lhx4) regulates retinal neural differentiation and visual function in
499 zebrafish. *Sci Rep* **11**, (2021).

500 73. Abdo, H. *et al.* Dependence on the transcription factor Shox2 for specification of sensory neurons
501 conveying discriminative touch. *European Journal of Neuroscience* **34**, 1529–1541 (2011).

502

503

504

505

506

507

508

509

510

511

512

513

514 ## Figure Legends

515 **Figure 1. Temporally dynamic relative transcript expression during chick trigeminal ganglion**
516 **development. A)** Polar plot depicting relative temporal relationships of differentially expressed genes
517 detected in the HH13/14, HH15/16, and HH17/18 chick trigeminal ganglion. Individual genes are
518 represented as single points based on changes in expression across the three timepoints. In the three-
519 point angular profiles surrounding the circular plot, the left dot represents HH13/14, the middle dot
520 represents HH15/16, and the right dot represents HH17/18, whereas the pattern of each profile
521 demonstrates the relative relationship of a gene's expression at a given degree along the circular plot, i.e.
522 the yellow profile represents a gene that does not change from HH13/14 to HH15/16, but is significantly
523 upregulated from HH15/16 to HH17/18. Genes exhibiting a maximum Log_2 fold change deemed
524 significant ($p<0.05$ after Benjamini-Hochberg correction) at one timepoint relative to at least one other
525 (three total comparisons) are shown. Maximal Log_2 fold change for each gene is represented as distance
526 from the center, while the concentric dotted lines represent Log_2 fold change thresholds of 0, 2, and 4,
527 respectively, from the center of the plot moving outward. Gray bars around the outer circumference
528 demonstrate the number of genes at any given degree along the circle, which are transformed to a
529 straight axis in B. **B)** Color-coded histogram illustrating the number of genes at any given degree ("H")
530 along the circumference of the polar plot, where 0 degrees equates to the yellow three-point profile in A.

531

532 **Figure 2. Genes associated with neuron development and axon guidance are continuously**
533 **upregulated between HH13/14 and HH17/18 in the chick trigeminal ganglion. A)** The yellow wedge
534 overlayed on the polar plot represents the 60-degree angle used to define Sector 1 for gene ontology
535 enrichment. **B)** Color-coded line plots reveal the relative expression patterns of individual genes included
536 in Sector 1. The dotted line is the average scaled gene expression of all genes in Sector 1. **C-D)** Bar
537 graphs illustrate the fifteen most enriched biological processes (C) and cellular components (D)
538 associated with Sector 1 genes (Fisher's exact test), in order of transformed p-value. The box outlined to
539 the right lists all genes from Sector 1 associated with "Axonogenesis" (GO:0007409).

540

541 **Figure 3. Validation of protein and transcript expression of neuronal genes in Sector 1. A-C)**
542 Fluorescent immunohistochemistry on transverse sections taken through the forming chick HH18
543 trigeminal ganglion demonstrates interspersed Sox10-positive (green) and Islet1-positive (purple) nuclei,
544 confirming the presence of both neural crest cells and placodal neurons, respectively (A). Neurons
545 expressing either N-Cadherin (B, purple) or beta III tubulin ("Tubb3", C, purple) express protein products
546 of genes in Sector 1, including HuD (B, green) and Stmn2 (C, green). Arrows point to representative cells
547 that co-express N-Cadherin and HuD (B) or Tubb3 and Stmn2 (C). DAPI (blue) labels cell nuclei. **D)** *In*
548 *situ* hybridization data from the Allen Developing Brain Atlas showing expression of Sector 1 genes in the
549 E11.5 mouse trigeminal ganglion, including *Ntrk1* (https://developingmouse.brain-
550 map.org/experiment/show/100046577), *Cntn2* (https://developingmouse.brain-
551 map.org/experiment/show/100047095), and *Robo2* (https://developingmouse.brain-
552 map.org/experiment/show/100046870)[56]. Scale bar in A is 20μm for A-C and 250μm for D.

553

554 **Figure 4. Autophagy-related genes are upregulated from HH13/14 to HH15/16, and maintained at**
555 **HH17/18, in the chick trigeminal ganglion. A)** The green wedge overlayed on the polar plot represents
556 the 60-degree angle used to define Sector 2 for gene ontology enrichment. **B)** Color-coded line plots
557 reveal the relative expression patterns of individual genes included in Sector 2. The dotted line is the
558 average scaled gene expression of all genes in Sector 2. **C-D)** Bar graphs illustrate the fifteen most
559 enriched biological processes (C) and cellular components (D) associated with Sector 2 genes (Fisher's
560 exact test), organized by transformed p-value. The box outlined to the right lists all genes from Sector 2
561 associated with "Lysosomal Transport" (GO:0007041) and "Positive Regulation of Autophagy"
562 (GO:0010508).

563

564 **Supplemental Figures Legends**

565 **Supplemental Figure 1. Analyses of sample similarity and temporal relationships of genes related**
566 **to axonogenesis. A)** Results of principal component analysis comparing all biological and technical
567 replicates from HH13/14 (blue), HH15/16 (yellow), and HH17/18 (green) after normalization. Ellipses are
568 overlayed to demonstrate how samples within each staging bin cluster together on the plot. **B)** Heatmap
569 illustrating temporal expression patterns of genes associated with GO terms related to axonogenesis,
570 including "Axonogenesis", "Regulation of Axonogenesis", "Positive/Negative Regulation of Axonogenesis",
571 "CNS Neuron Axonogenesis", and "CNS Projection Neuron Axonogenesis". Heatmap depicts relative
572 expression at HH13/14 (left column), HH15/16 (middle column), and HH17/18 (right column), where blue
573 represents the minimum expression for a given row, red represents the maximum expression, and white
574 represents the mid-point between minimum and maximum expression. Brackets label the Polar Plot
575 Sector under which each group of genes falls.

576

577 **Supplemental Figure 2.** Sector 3 gene expression and ontologies. **A)** The light blue wedge overlayed on
578 the polar plot from Figure 1 represents the 60-degree angle used to define Sector 3 for gene ontology
579 enrichment. **B)** Color-coded line plots reveal the relative expression patterns of individual genes included
580 in Sector 3. The dotted line is the average scaled gene expression of all genes in Sector 3. **C-D)** Bar
581 graphs illustrate the fifteen most enriched biological processes (C) and cellular components (D)
582 associated with Sector 3 genes (Fisher's exact test), organized by transformed p-value.

583

584 **Supplemental Figure 3.** Sector 4 gene expression and ontologies. **A)** The dark blue wedge overlayed on
585 the polar plot from Figure 1 represents the 60-degree angle used to define Sector 4 for gene ontology
586 enrichment. **B)** Color-coded line plots reveal the relative expression patterns of individual genes included
587 in Sector 4. The dotted line is the average scaled gene expression of all genes in Sector 4. **C-D)** Bar
588 graphs illustrate the fifteen most enriched biological processes (C) and cellular components (D)
589 associated with Sector 4 genes (Fisher's exact test), organized by transformed p-value.

590

591 **Supplemental Figure 4.** Sector 5 gene expression and ontologies. **A)** The pink wedge overlayed on the
592 polar plot from Figure 1 represents the 60-degree angle used to define Sector 5 for gene ontology
593 enrichment. **B)** Color-coded line plots reveal the relative expression patterns of individual genes included
594 in Sector 5. The dotted line is the average scaled gene expression of all genes in Sector 5. **C-D)** Bar
595 graphs illustrate the fifteen most enriched biological processes (C) and cellular components (D)
596 associated with Sector 5 genes (Fisher's exact test), organized by transformed p-value.

597

598 **Supplemental Figure 5.** Sector 6 gene expression and ontologies. **A)** The orange wedge overlayed on
599 the polar plot from Figure 1 represents the 60-degree angle used to define Sector 6 for gene ontology
600 enrichment. **B)** Color-coded line plots reveal the relative expression patterns of individual genes included
601 in Sector 6. The dotted line is the average scaled gene expression of all genes in Sector 6. **C-D)** Bar
602 graphs illustrate the fifteen most enriched biological processes (C) and cellular components (D)
603 associated with Sector 6 genes (Fisher's exact test), organized by transformed p-value.

604

605 **Supplemental Data Files**

606 **Supplemental File 1.** Color-coded Excel spreadsheet containing calculated values for differential
607 expression comparisons and polar plot.

608

609 **Supplemental File 2.** Excel spreadsheets compiling gene ontology enrichment results for Biological
610 Processes (BP) and Cellular Components (CC) associated with each 60-degree polar plot sector.

A

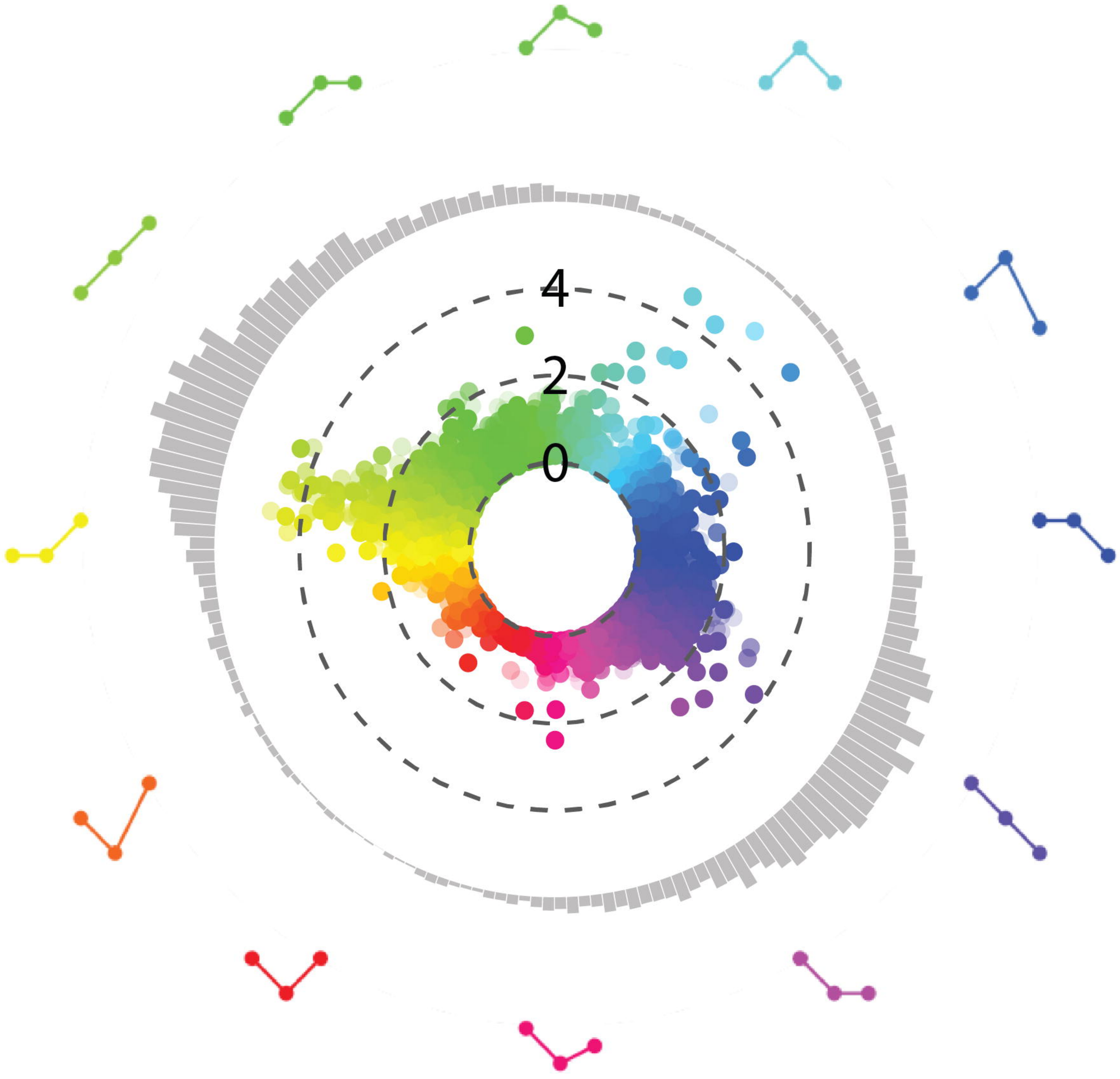
4
2
0

B

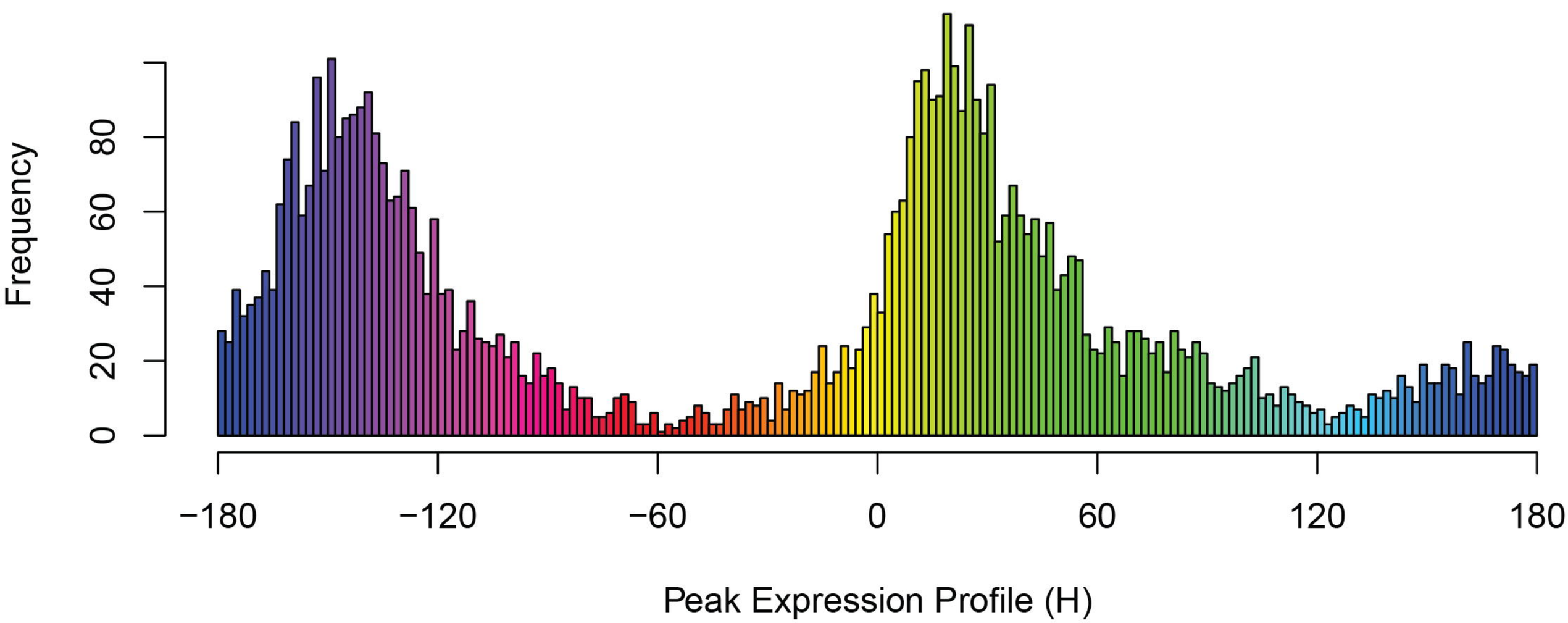
Frequency
0
20
40
60
80
−180
−120
−60
0
60
120
180
Peak Expression Profile (H)

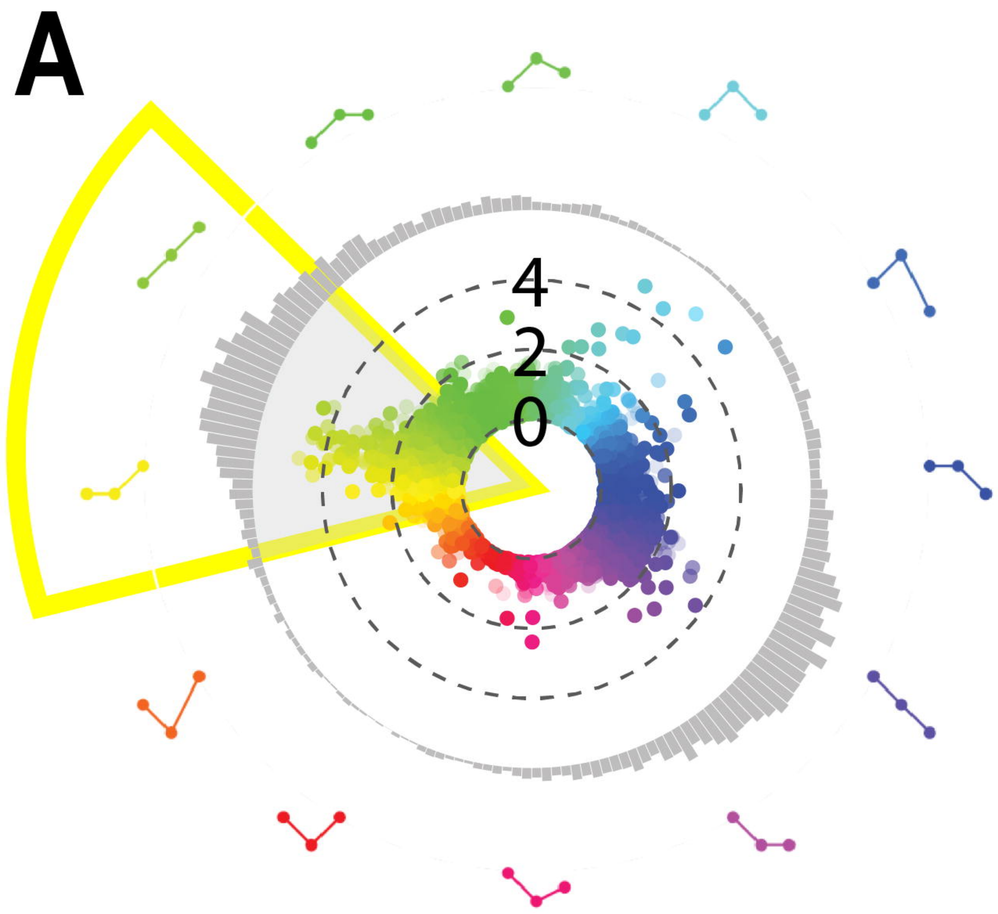
A
4
2
0

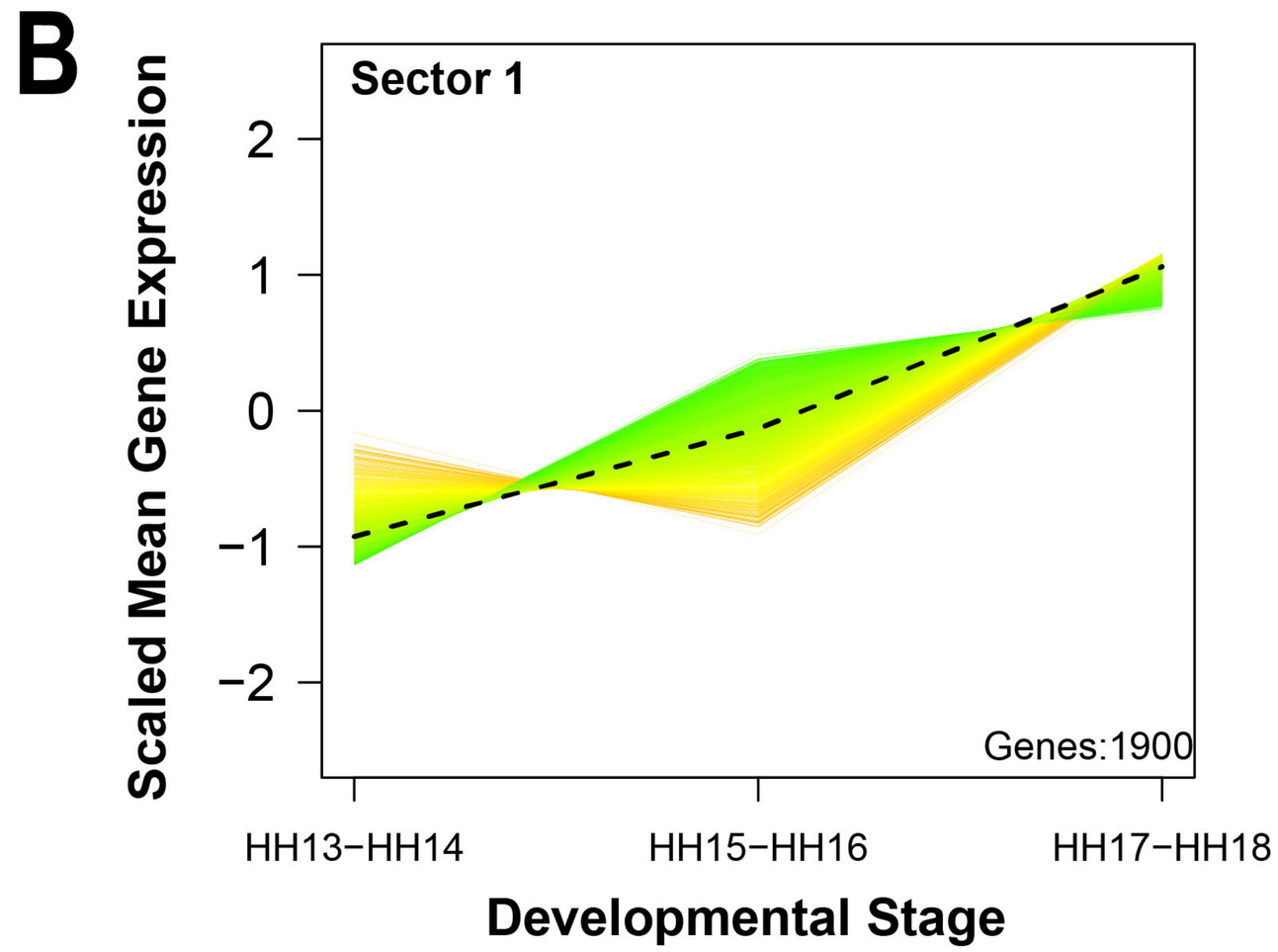
B
Sector 1
Scaled Mean Gene Expression
2
1
0
−1
−2
Genes:1900
HH13−HH14
HH15−HH16
HH17−HH18
Developmental Stage

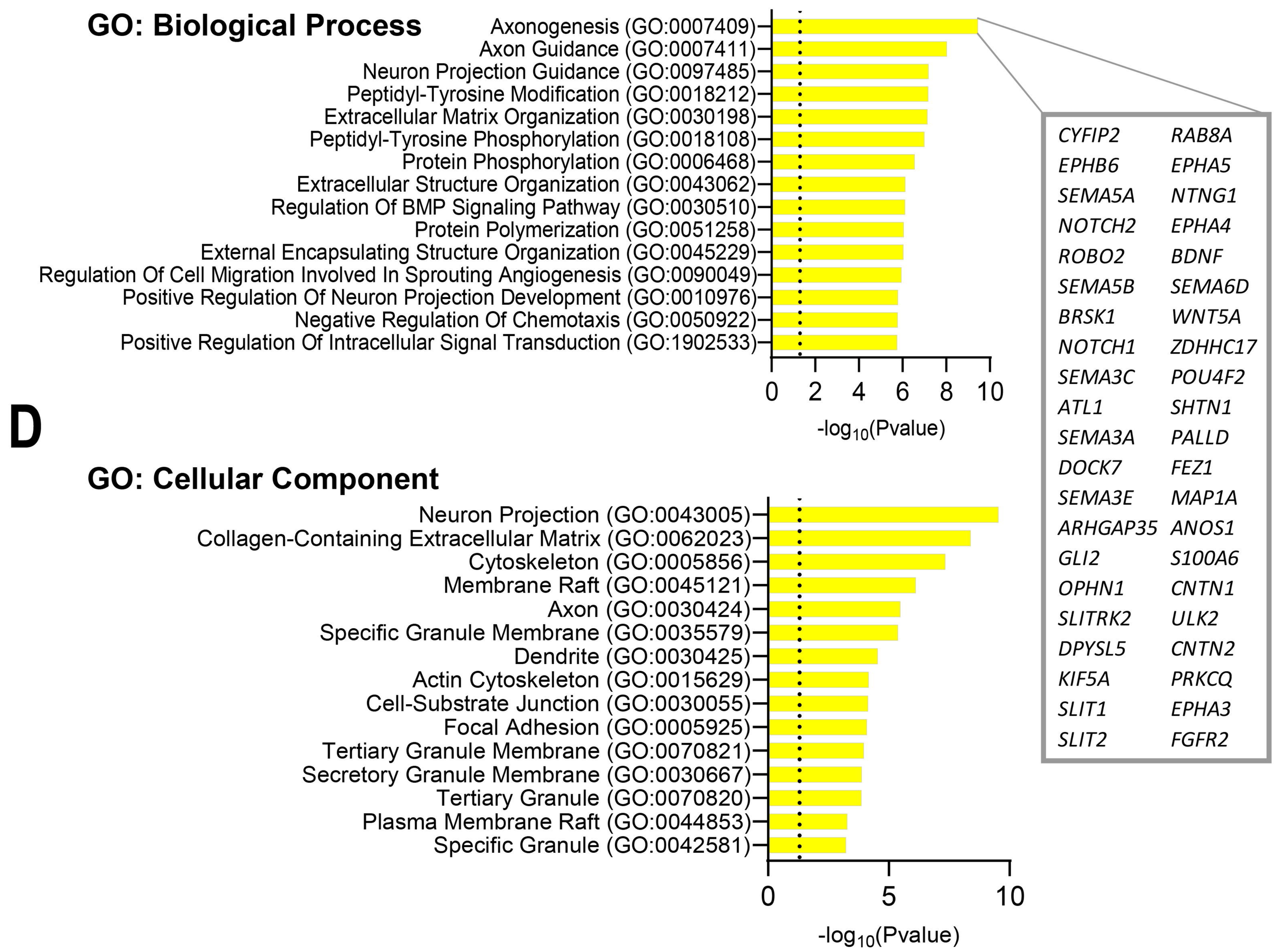
C
GO: Biological Process
Axonogenesis (GO:0007409)
Axon Guidance (GO:0007411)
Neuron Projection Guidance (GO:0097485)
Peptidyl-Tyrosine Modification (GO:0018212)
Extracellular Matrix Organization (GO:0030198)
Peptidyl-Tyrosine Phosphorylation (GO:0018108)
Protein Phosphorylation (GO:0006468)
Extracellular Structure Organization (GO:0043062)
Regulation Of BMP Signaling Pathway (GO:0030510)
Protein Polymerization (GO:0051258)
External Encapsulating Structure Organization (GO:0045229)
Regulation Of Cell Migration Involved In Sprouting Angiogenesis (GO:0090049)
Positive Regulation Of Neuron Projection Development (GO:0010976)
Negative Regulation Of Chemotaxis (GO:0050922)
Positive Regulation Of Intracellular Signal Transduction (GO:1902533)
0 2 4 6 8 10
-log10(Pvalue)
CYFIP2 RAB8A
EPHB6 EPHA5
SEMA5A NTNG1
NOTCH2 EPHA4
ROBO2 BDNF
SEMA5B SEMA6D
BRSK1 WNT5A
NOTCH1 ZDHHC17
SEMA3C POU4F2
ATL1 SHTN1
SEMA3A PALLD
DOCK7 FEZ1
SEMA3E MAP1A
ARHGAP35 ANOS1
GLI2 S100A6
OPHN1 CNTN1
SLITRK2 ULK2
DPYSL5 CNTN2
KIF5A PRKCQ
SLIT1 EPHA3
SLIT2 FGFR2
D
GO: Cellular Component
Neuron Projection (GO:0043005)
Collagen-Containing Extracellular Matrix (GO:0062023)
Cytoskeleton (GO:0005856)
Membrane Raft (GO:0045121)
Axon (GO:0030424)
Specific Granule Membrane (GO:0035579)
Dendrite (GO:0030425)
Actin Cytoskeleton (GO:0015629)
Cell-Substrate Junction (GO:0030055)
Focal Adhesion (GO:0005925)
Tertiary Granule Membrane (GO:0070821)
Secretory Granule Membrane (GO:0030667)
Tertiary Granule (GO:0070820)
Plasma Membrane Raft (GO:0044853)
Specific Granule (GO:0042581)
0 5 10
-log10(Pvalue)

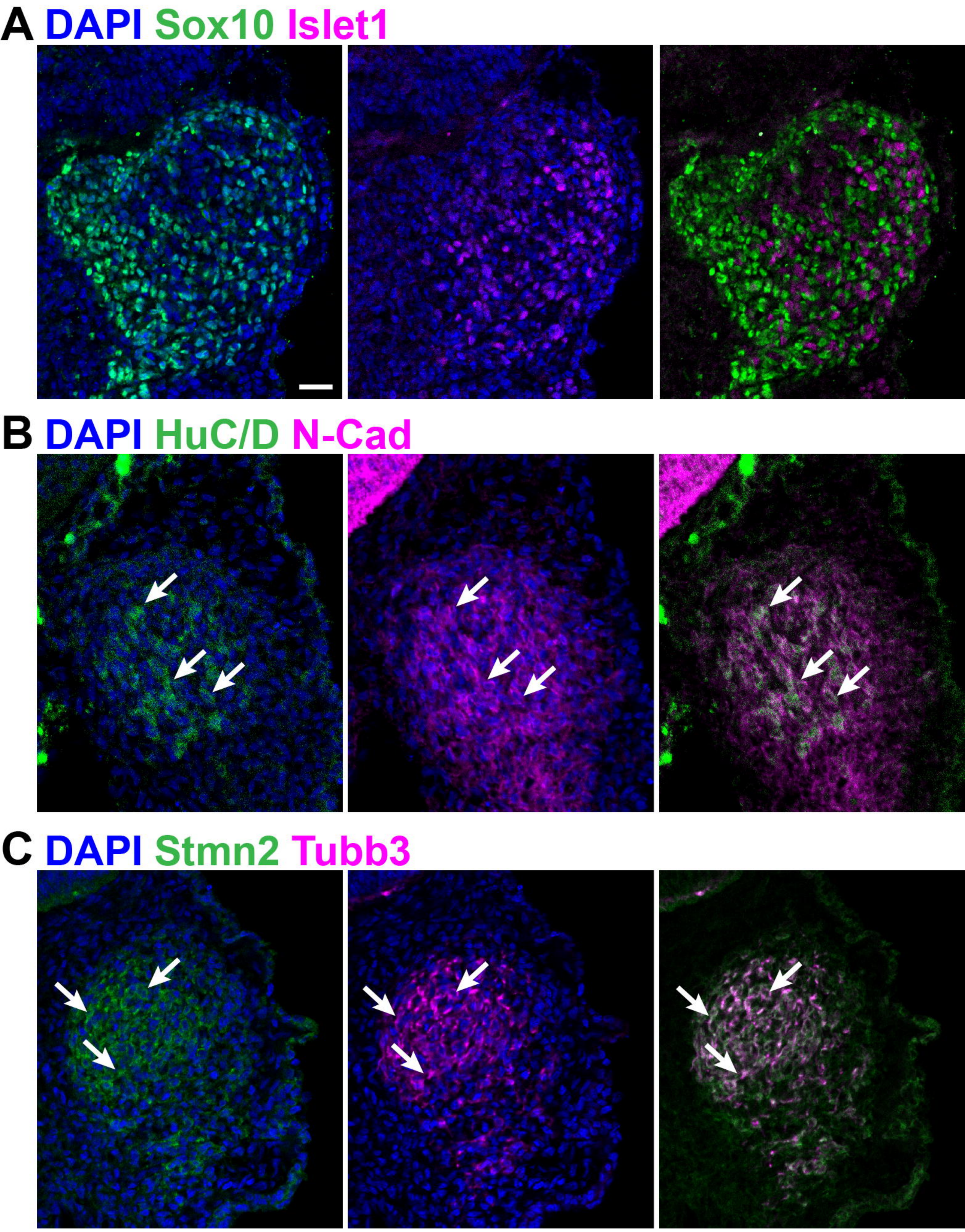
A DAPI Sox10 Islet1
B DAPI HuC/D N-Cad
C DAPI Stmn2 Tubb3
D E11.5 mouse
Ntrk1
Cntn2
Robo2

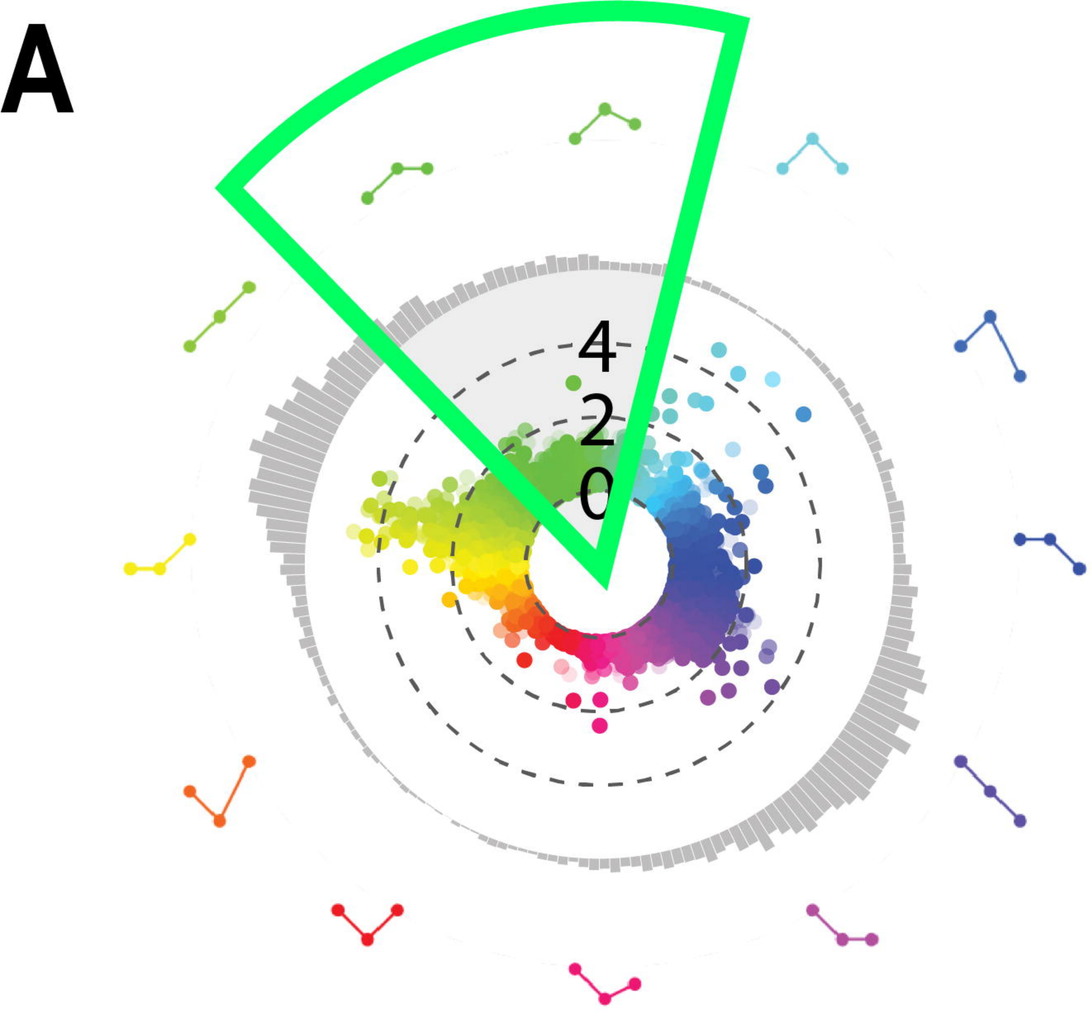
A
4
2
0

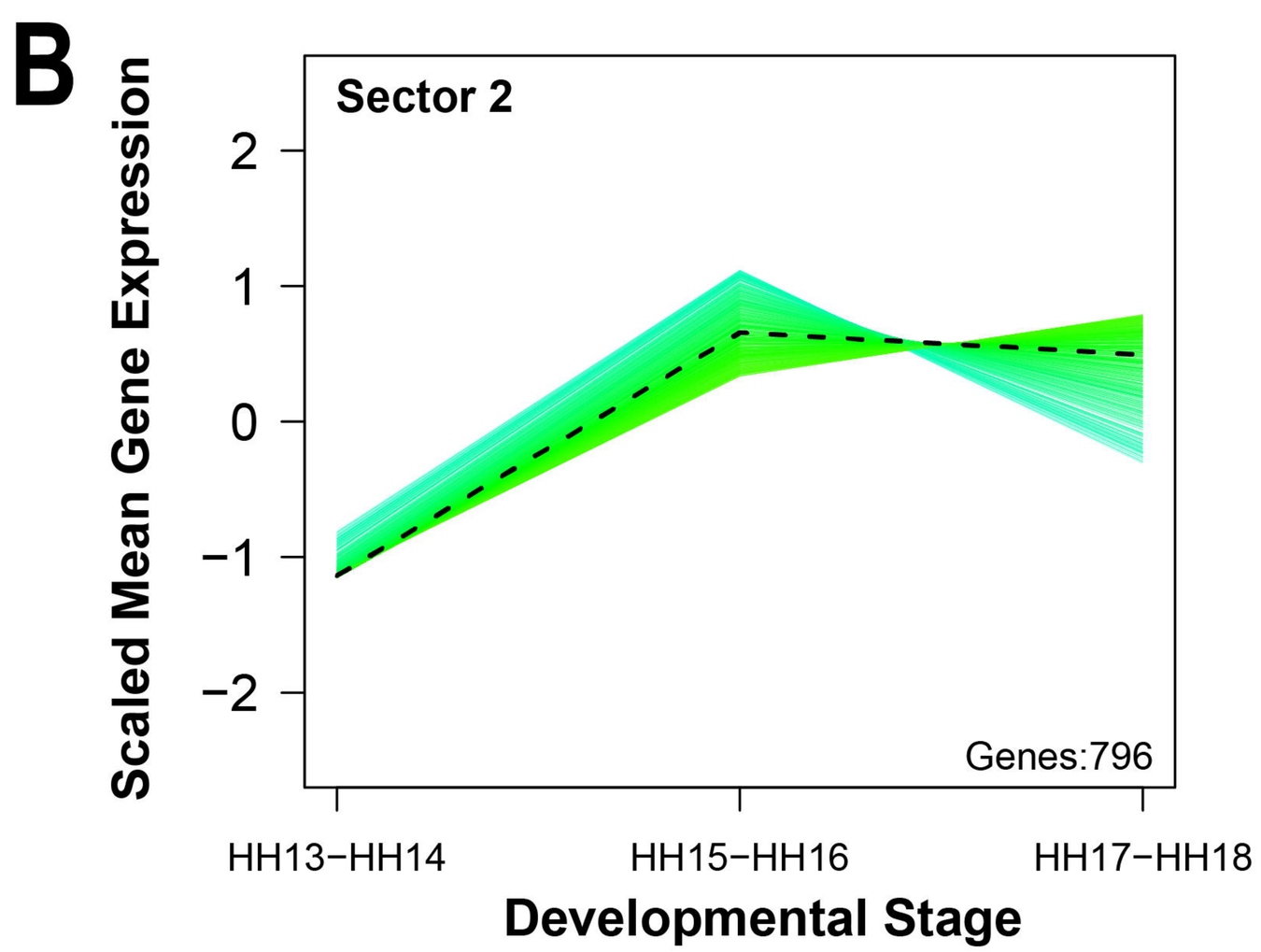
B
Sector 2
Scaled Mean Gene Expression
2
1
0
−1
−2
Genes:796
HH13−HH14
HH15−HH16
HH17−HH18
Developmental Stage

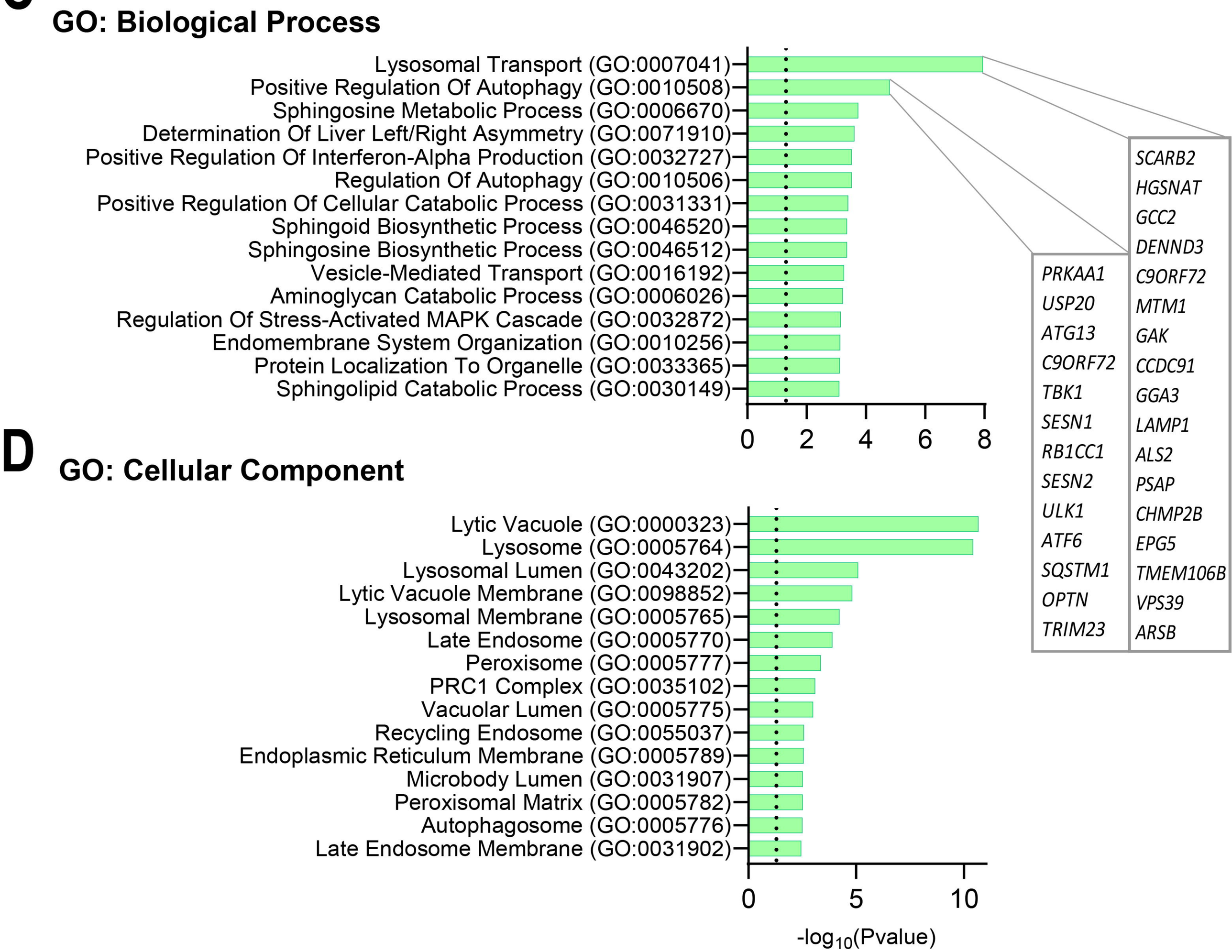
C
GO: Biological Process
Lysosomal Transport (GO:0007041)
Positive Regulation Of Autophagy (GO:0010508)
Sphingosine Metabolic Process (GO:0006670)
Determination Of Liver Left/Right Asymmetry (GO:0071910)
Positive Regulation Of Interferon-Alpha Production (GO:0032727)
Regulation Of Autophagy (GO:0010506)
Positive Regulation Of Cellular Catabolic Process (GO:0031331)
Sphingoid Biosynthetic Process (GO:0046520)
Sphingosine Biosynthetic Process (GO:0046512)
Vesicle-Mediated Transport (GO:0016192)
Aminoglycan Catabolic Process (GO:0006026)
Regulation Of Stress-Activated MAPK Cascade (GO:0032872)
Endomembrane System Organization (GO:0010256)
Protein Localization To Organelle (GO:0033365)
Sphingolipid Catabolic Process (GO:0030149)
0
2
4
6
8
PRKAA1
USP20
ATG13
C9ORF72
TBK1
SESN1
RB1CC1
SESN2
ULK1
ATF6
SQSTM1
OPTN
TRIM23
SCARB2
HGSNAT
GCC2
DENND3
C9ORF72
MTM1
GAK
CCDC91
GGA3
LAMP1
ALS2
PSAP
CHMP2B
EPG5
TMEM106B
VPS39
ARSB
D
GO: Cellular Component
Lytic Vacuole (GO:0000323)
Lysosome (GO:0005764)
Lysosomal Lumen (GO:0043202)
Lytic Vacuole Membrane (GO:0098852)
Lysosomal Membrane (GO:0005765)
Late Endosome (GO:0005770)
Peroxisome (GO:0005777)
PRC1 Complex (GO:0035102)
Vacuolar Lumen (GO:0005775)
Recycling Endosome (GO:0055037)
Endoplasmic Reticulum Membrane (GO:0005789)
Microbody Lumen (GO:0031907)
Peroxisomal Matrix (GO:0005782)
Autophagosome (GO:0005776)
Late Endosome Membrane (GO:0031902)
0
5
10
-log10(Pvalue)

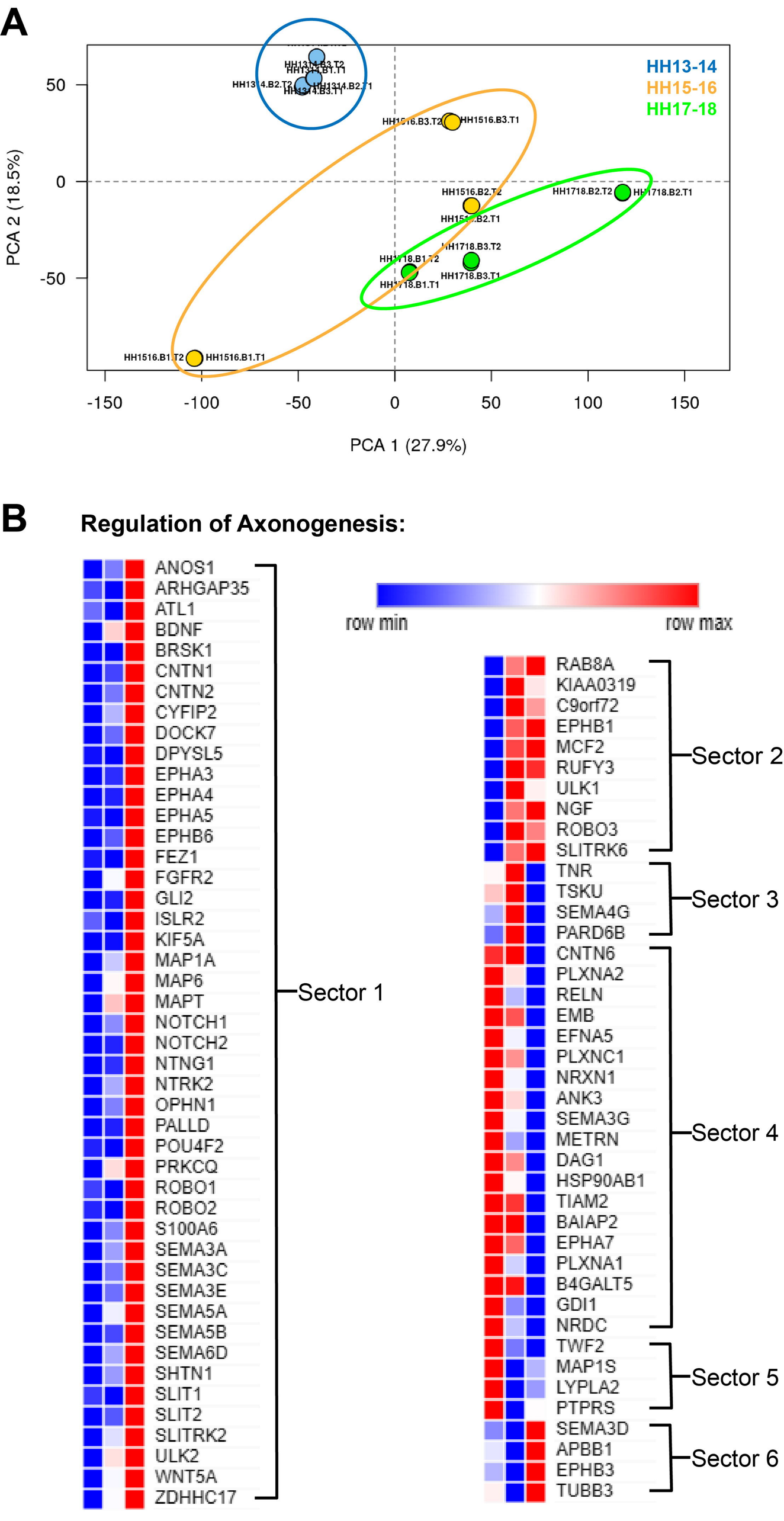
A
HH13-14
HH15-16
HH17-18
PCA 2 (18.5%)
PCA 1 (27.9%)
50
0
-50
-150
-100
-50
0
50
100
150
HH1516.B3.T2
HH1516.B3.T1
HH1516.B2.T2
HH1718.B2.T2
HH1718.B2.T1
HH1718.B3.T2
HH1718.B3.T1
HH1516.B1.T2
HH1516.B1.T1
B
Regulation of Axonogenesis:
row min
row max
ANOS1
ARHGAP35
ATL1
BDNF
BRSK1
CNTN1
CNTN2
CYFIP2
DOCK7
DPYSL5
EPHA3
EPHA4
EPHA5
EPHB6
FEZ1
FGFR2
GLI2
ISLR2
KIF5A
MAP1A
MAP6
MAPT
NOTCH1
NOTCH2
NTNG1
NTRK2
OPHN1
PALLD
POU4F2
PRKCQ
ROBO1
ROBO2
S100A6
SEMA3A
SEMA3C
SEMA3E
SEMA5A
SEMA5B
SEMA6D
SHTN1
SLIT1
SLIT2
SLITRK2
ULK2
WNT5A
ZDHHC17
Sector 1
RAB8A
KIAA0319
C9orf72
EPHB1
MCF2
RUFY3
ULK1
NGF
ROBO3
SLITRK6
Sector 2
TNR
TSKU
SEMA4G
PARD6B
Sector 3
CNTN6
PLXNA2
RELN
EMB
EFNA5
PLXNC1
NRXN1
ANK3
SEMA3G
METRN
DAG1
HSP90AB1
TIAM2
BAIAP2
EPHA7
PLXNA1
B4GALT5
GDI1
NRDC
Sector 4
TWF2
MAP1S
LYPLA2
PTPRS
Sector 5
SEMA3D
APBB1
EPHB3
TUBB3
Sector 6

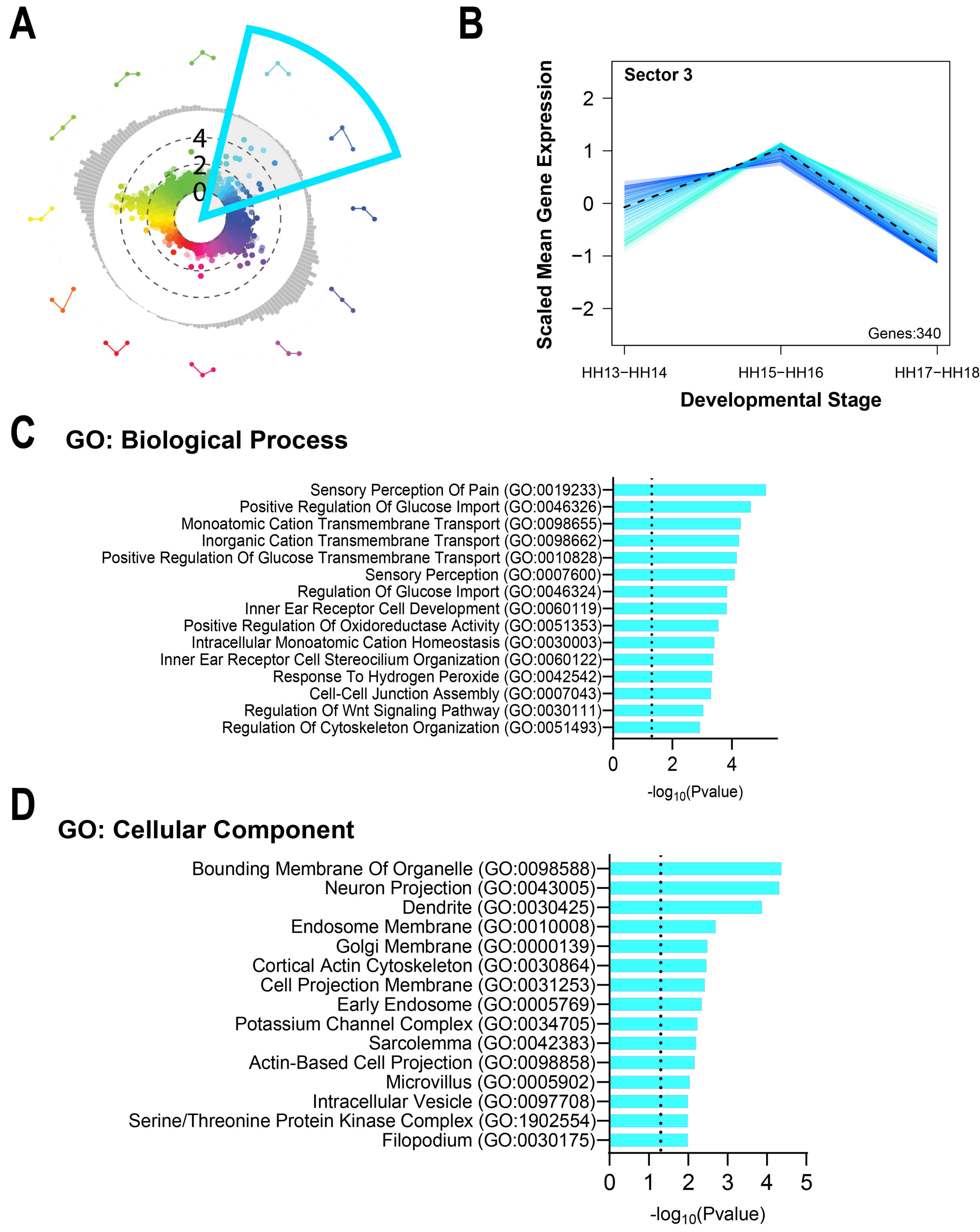
A
4
2
0
B
Sector 3
Scaled Mean Gene Expression
2
1
0
−1
−2
Genes:340
HH13−HH14
HH15−HH16
HH17−HH18
Developmental Stage
C
GO: Biological Process
Sensory Perception Of Pain (GO:0019233)
Positive Regulation Of Glucose Import (GO:0046326)
Monoatomic Cation Transmembrane Transport (GO:0098655)
Inorganic Cation Transmembrane Transport (GO:0098662)
Positive Regulation Of Glucose Transmembrane Transport (GO:0010828)
Sensory Perception (GO:0007600)
Regulation Of Glucose Import (GO:0046324)
Inner Ear Receptor Cell Development (GO:0060119)
Positive Regulation Of Oxidoreductase Activity (GO:0051353)
Intracellular Monoatomic Cation Homeostasis (GO:0030003)
Inner Ear Receptor Cell Stereocilium Organization (GO:0060122)
Response To Hydrogen Peroxide (GO:0042542)
Cell-Cell Junction Assembly (GO:0007043)
Regulation Of Wnt Signaling Pathway (GO:0030111)
Regulation Of Cytoskeleton Organization (GO:0051493)
0
2
4
-log10(Pvalue)
D
GO: Cellular Component
Bounding Membrane Of Organelle (GO:0098588)
Neuron Projection (GO:0043005)
Dendrite (GO:0030425)
Endosome Membrane (GO:0010008)
Golgi Membrane (GO:0000139)
Cortical Actin Cytoskeleton (GO:0030864)
Cell Projection Membrane (GO:0031253)
Early Endosome (GO:0005769)
Potassium Channel Complex (GO:0034705)
Sarcolemma (GO:0042383)
Actin-Based Cell Projection (GO:0098858)
Microvillus (GO:0005902)
Intracellular Vesicle (GO:0097708)
Serine/Threonine Protein Kinase Complex (GO:1902554)
Filopodium (GO:0030175)
0
1
2
3
4
5
-log10(Pvalue)

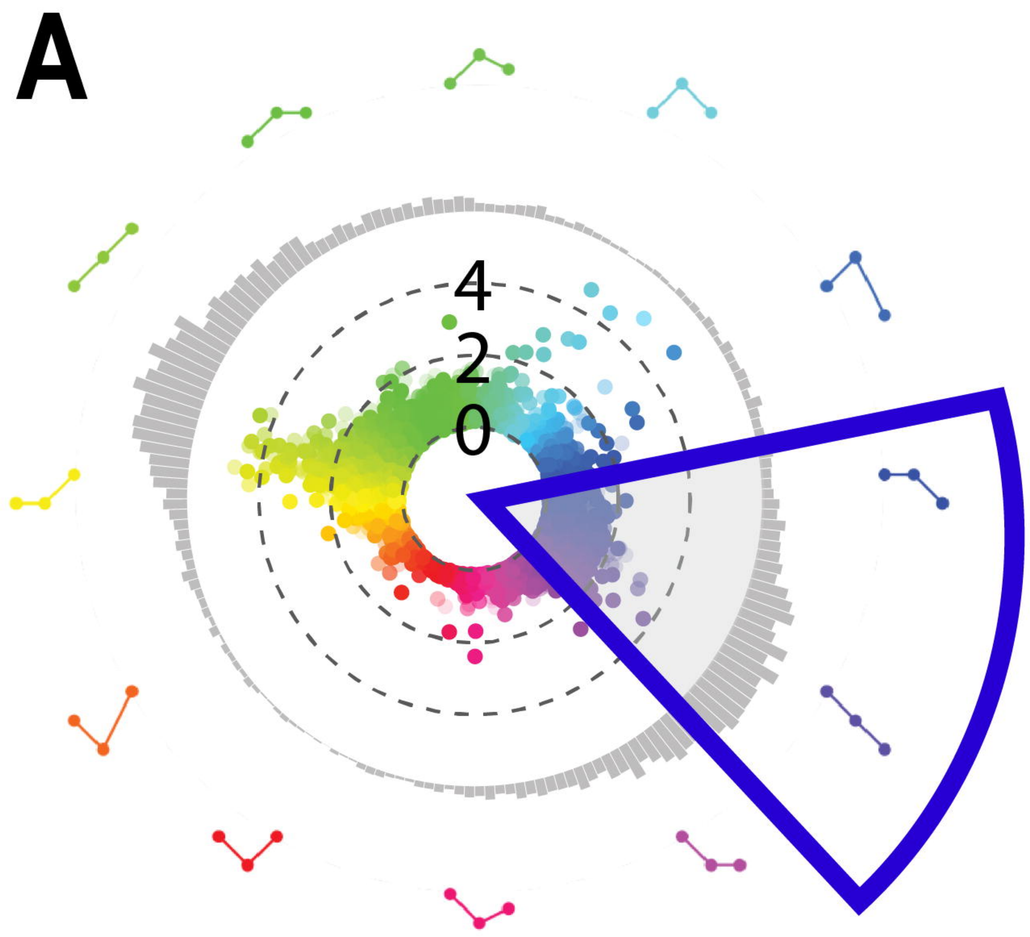
A
4
2
0

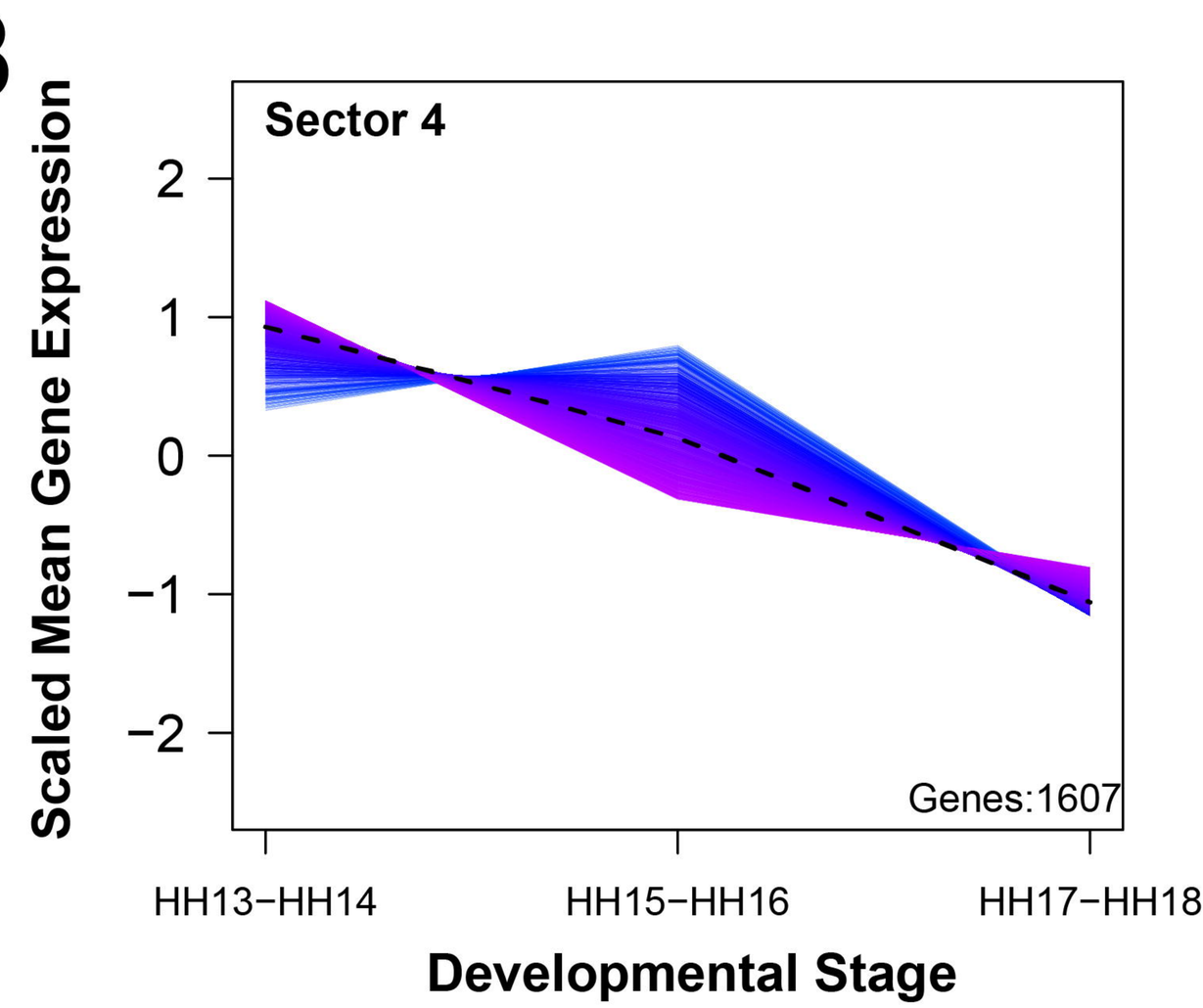
B
Sector 4
Scaled Mean Gene Expression
2
1
0
−1
−2
Genes:1607
HH13−HH14
HH15−HH16
HH17−HH18
Developmental Stage

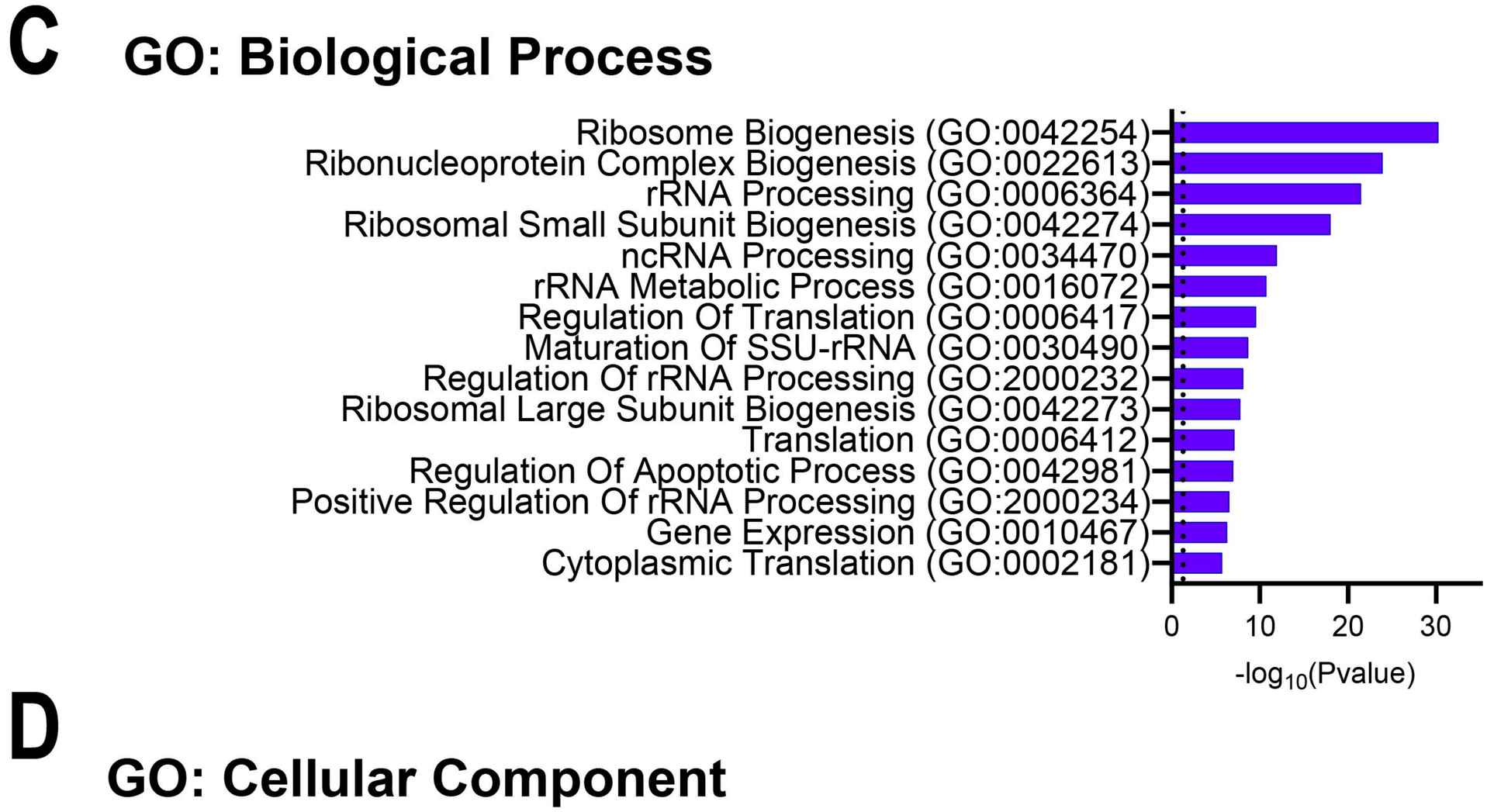
C
GO: Biological Process
Ribosome Biogenesis (GO:0042254)
Ribonucleoprotein Complex Biogenesis (GO:0022613)
rRNA Processing (GO:0006364)
Ribosomal Small Subunit Biogenesis (GO:0042274)
ncRNA Processing (GO:0034470)
rRNA Metabolic Process (GO:0016072)
Regulation Of Translation (GO:0006417)
Maturation Of SSU-rRNA (GO:0030490)
Regulation Of rRNA Processing (GO:2000232)
Ribosomal Large Subunit Biogenesis (GO:0042273)
Translation (GO:0006412)
Regulation Of Apoptotic Process (GO:0042981)
Positive Regulation Of rRNA Processing (GO:2000234)
Gene Expression (GO:0010467)
Cytoplasmic Translation (GO:0002181)
0
10
20
30
-log10(Pvalue)

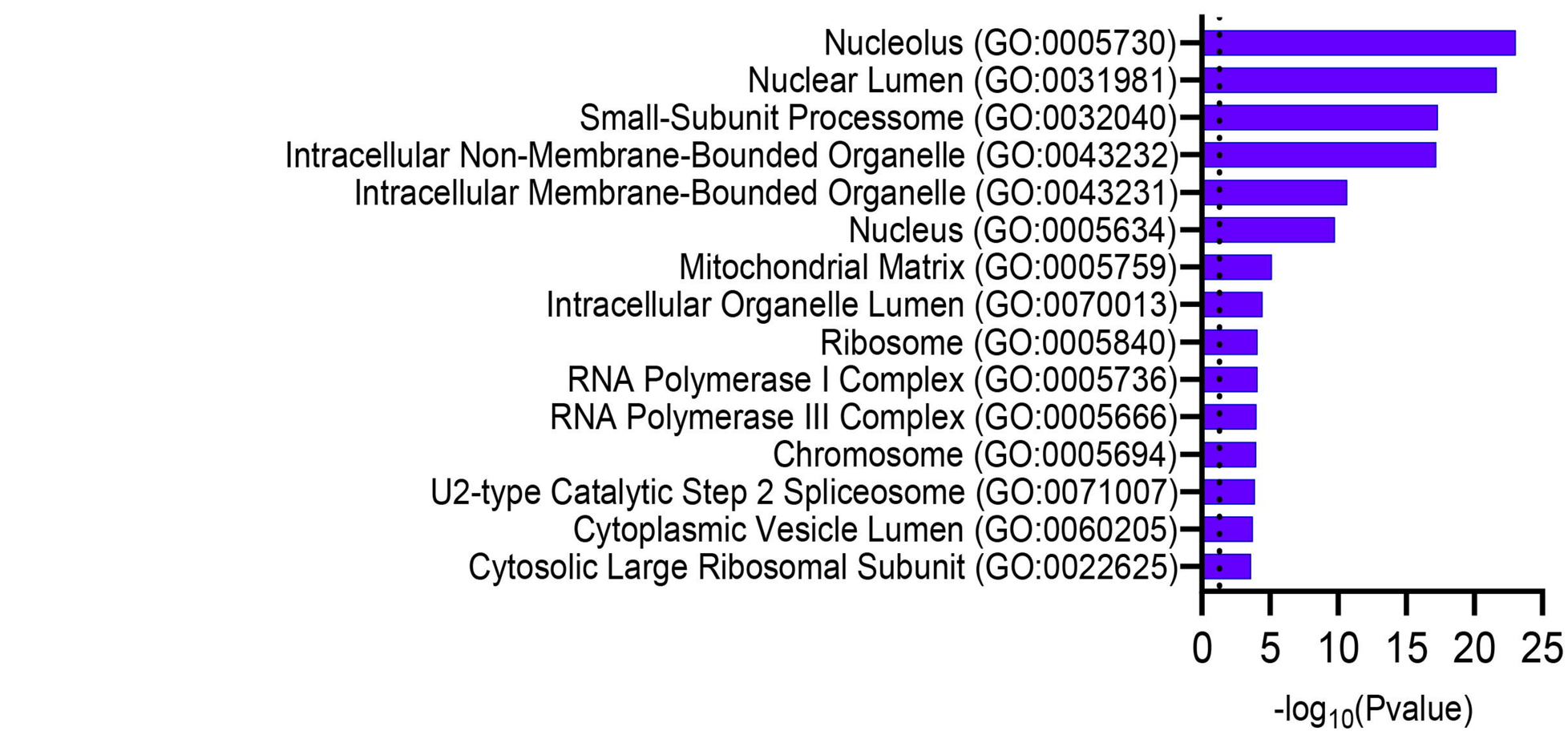
D
GO: Cellular Component
Nucleolus (GO:0005730)
Nuclear Lumen (GO:0031981)
Small-Subunit Processome (GO:0032040)
Intracellular Non-Membrane-Bounded Organelle (GO:0043232)
Intracellular Membrane-Bounded Organelle (GO:0043231)
Nucleus (GO:0005634)
Mitochondrial Matrix (GO:0005759)
Intracellular Organelle Lumen (GO:0070013)
Ribosome (GO:0005840)
RNA Polymerase I Complex (GO:0005736)
RNA Polymerase III Complex (GO:0005666)
Chromosome (GO:0005694)
U2-type Catalytic Step 2 Spliceosome (GO:0071007)
Cytoplasmic Vesicle Lumen (GO:0060205)
Cytosolic Large Ribosomal Subunit (GO:0022625)
0
5
10
15
20
25
-log10(Pvalue)

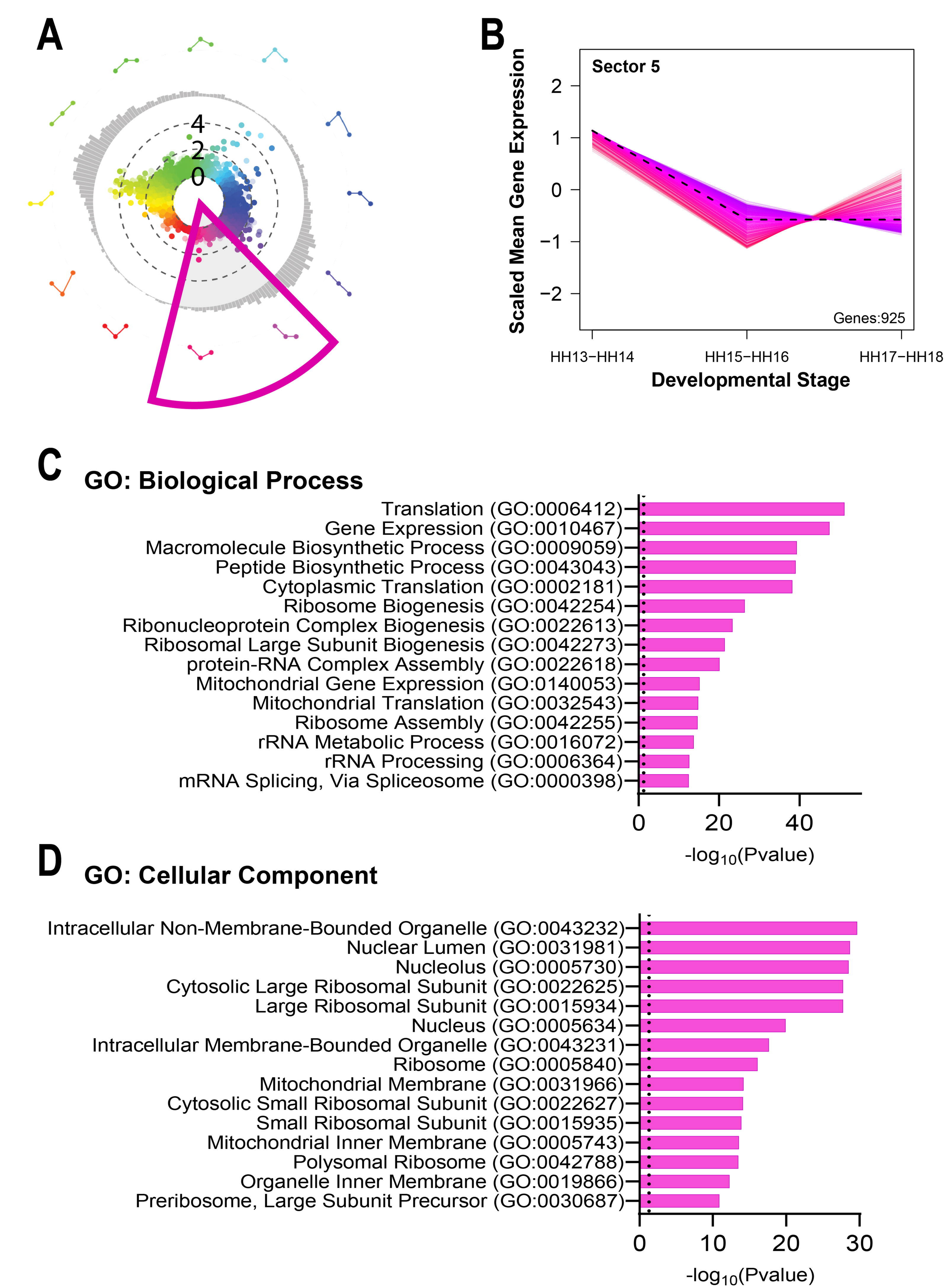
A
4
2
0
B
Sector 5
Scaled Mean Gene Expression
2
1
0
−1
−2
Genes:925
HH13−HH14
HH15−HH16
HH17−HH18
Developmental Stage
C
GO: Biological Process
Translation (GO:0006412)
Gene Expression (GO:0010467)
Macromolecule Biosynthetic Process (GO:0009059)
Peptide Biosynthetic Process (GO:0043043)
Cytoplasmic Translation (GO:0002181)
Ribosome Biogenesis (GO:0042254)
Ribonucleoprotein Complex Biogenesis (GO:0022613)
Ribosomal Large Subunit Biogenesis (GO:0042273)
protein-RNA Complex Assembly (GO:0022618)
Mitochondrial Gene Expression (GO:0140053)
Mitochondrial Translation (GO:0032543)
Ribosome Assembly (GO:0042255)
rRNA Metabolic Process (GO:0016072)
rRNA Processing (GO:0006364)
mRNA Splicing, Via Spliceosome (GO:0000398)
0
20
40
-log10(Pvalue)
D
GO: Cellular Component
Intracellular Non-Membrane-Bounded Organelle (GO:0043232)
Nuclear Lumen (GO:0031981)
Nucleolus (GO:0005730)
Cytosolic Large Ribosomal Subunit (GO:0022625)
Large Ribosomal Subunit (GO:0015934)
Nucleus (GO:0005634)
Intracellular Membrane-Bounded Organelle (GO:0043231)
Ribosome (GO:0005840)
Mitochondrial Membrane (GO:0031966)
Cytosolic Small Ribosomal Subunit (GO:0022627)
Small Ribosomal Subunit (GO:0015935)
Mitochondrial Inner Membrane (GO:0005743)
Polysomal Ribosome (GO:0042788)
Organelle Inner Membrane (GO:0019866)
Preribosome, Large Subunit Precursor (GO:0030687)
0
10
20
30
-log10(Pvalue)

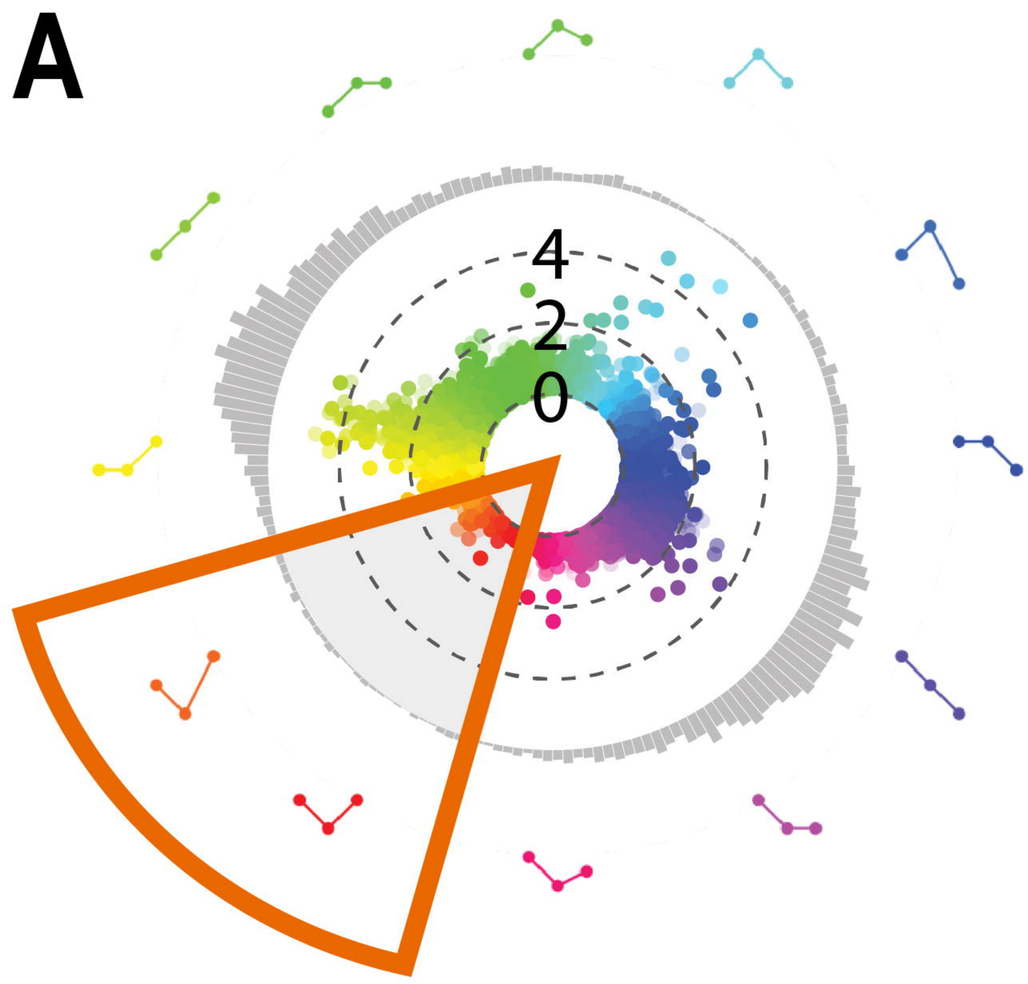
A
4
2
0

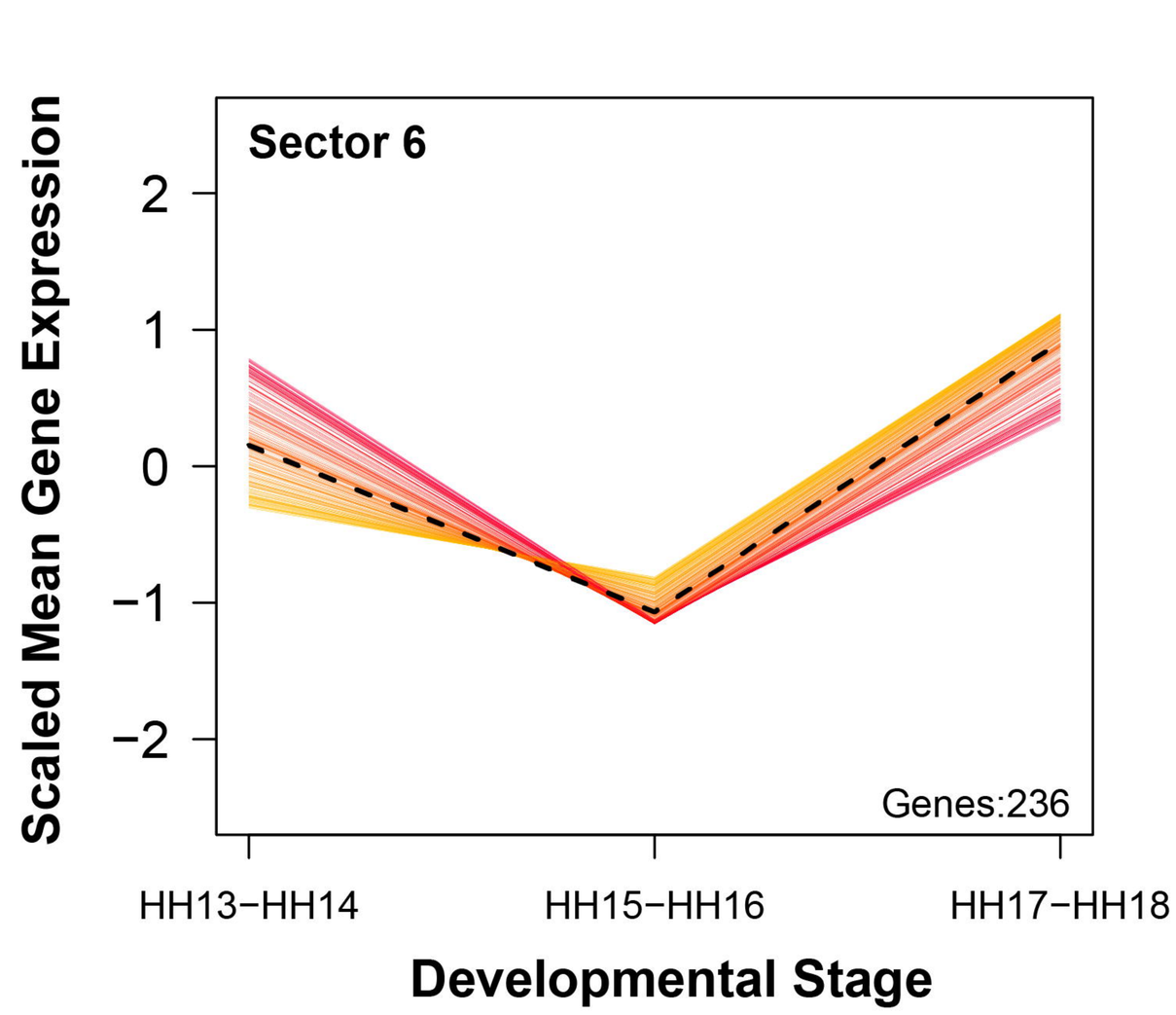
B
Sector 6
Genes:236
Scaled Mean Gene Expression
2
1
0
−1
−2
HH13−HH14
HH15−HH16
HH17−HH18
Developmental Stage

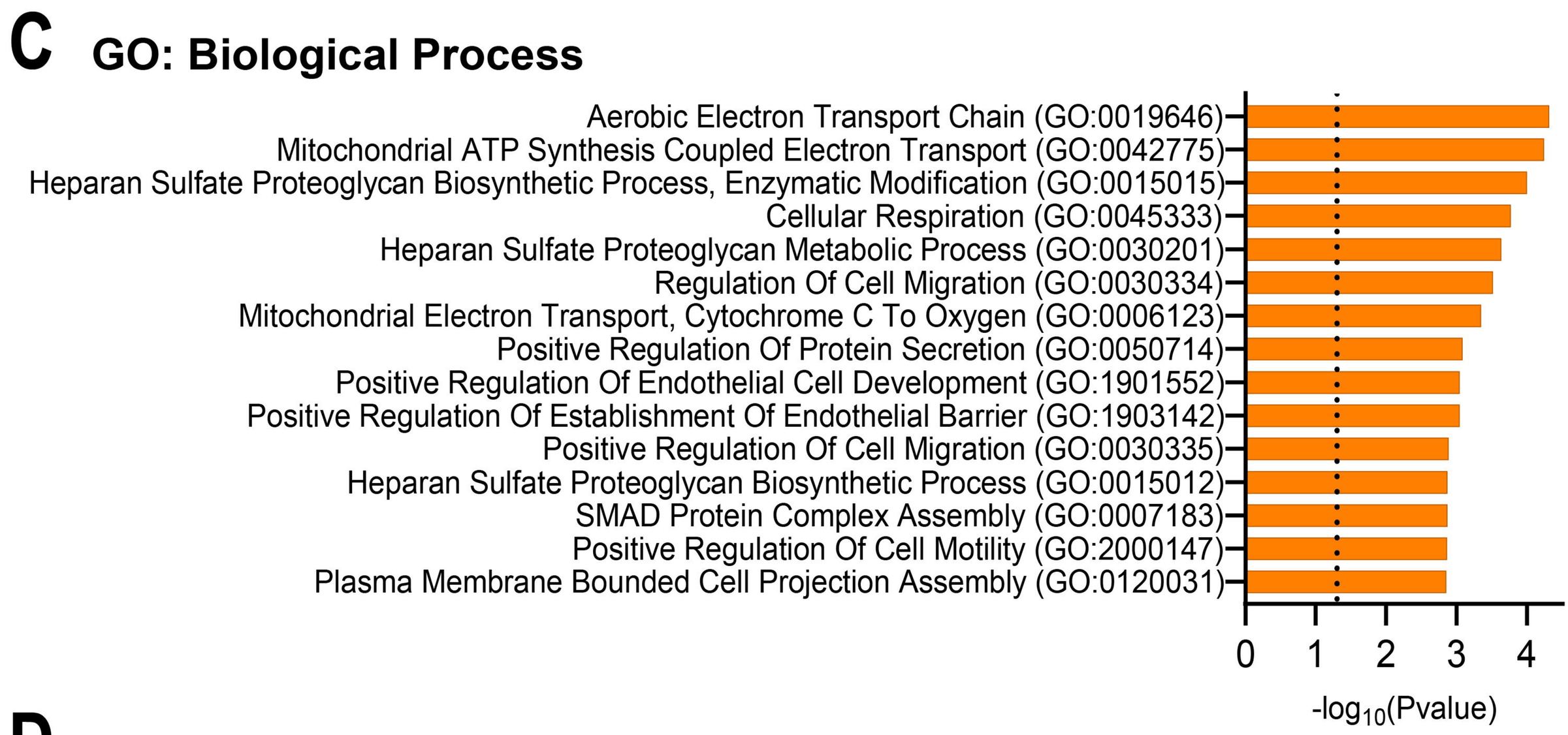
C
GO: Biological Process
Aerobic Electron Transport Chain (GO:0019646)
Mitochondrial ATP Synthesis Coupled Electron Transport (GO:0042775)
Heparan Sulfate Proteoglycan Biosynthetic Process, Enzymatic Modification (GO:0015015)
Cellular Respiration (GO:0045333)
Heparan Sulfate Proteoglycan Metabolic Process (GO:0030201)
Regulation Of Cell Migration (GO:0030334)
Mitochondrial Electron Transport, Cytochrome C To Oxygen (GO:0006123)
Positive Regulation Of Protein Secretion (GO:0050714)
Positive Regulation Of Endothelial Cell Development (GO:1901552)
Positive Regulation Of Establishment Of Endothelial Barrier (GO:1903142)
Positive Regulation Of Cell Migration (GO:0030335)
Heparan Sulfate Proteoglycan Biosynthetic Process (GO:0015012)
SMAD Protein Complex Assembly (GO:0007183)
Positive Regulation Of Cell Motility (GO:2000147)
Plasma Membrane Bounded Cell Projection Assembly (GO:0120031)
0
1
2
3
4
-log10(Pvalue)

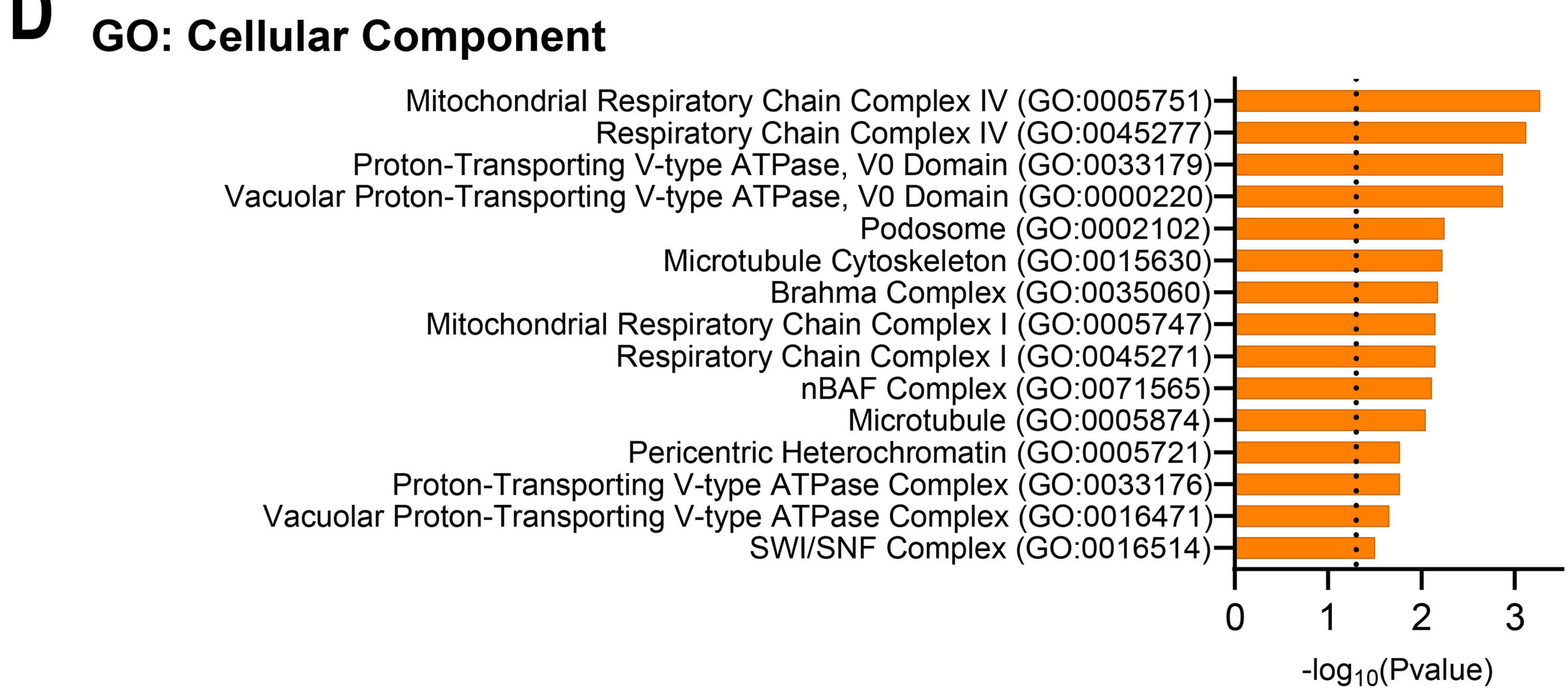
D
GO: Cellular Component
Mitochondrial Respiratory Chain Complex IV (GO:0005751)
Respiratory Chain Complex IV (GO:0045277)
Proton-Transporting V-type ATPase, V0 Domain (GO:0033179)
Vacuolar Proton-Transporting V-type ATPase, V0 Domain (GO:0000220)
Podosome (GO:0002102)
Microtubule Cytoskeleton (GO:0015630)
Brahma Complex (GO:0035060)
Mitochondrial Respiratory Chain Complex I (GO:0005747)
Respiratory Chain Complex I (GO:0045271)
nBAF Complex (GO:0071565)
Microtubule (GO:0005874)
Pericentric Heterochromatin (GO:0005721)
Proton-Transporting V-type ATPase Complex (GO:0033176)
Vacuolar Proton-Transporting V-type ATPase Complex (GO:0016471)
SWI/SNF Complex (GO:0016514)
0
1
2
3
-log10(Pvalue)